Sensitivity of Ride Comfort

of a Motorcycle to the Rear Powertrain Mounting System

by

Brennan Long

A Report Submitted to the Faculty of the

Milwaukee School of Engineering

In Partial Fulfillment of the

Requirements for the Degree of

Master of Science in Engineering

Milwaukee, Wisconsin

May 2025

Abstract

The purpose of this Milwaukee School of Engineering (MSOE) Master of Science in Engineering (MSE) Capstone Project Report is to present the results of a project featuring a multi-degree-of-freedom planar model of a motorcycle with an isolated powertrain to investigate the sensitivity of ride comfort to the rear powertrain mounting system with a specific focus on the mounting system's stiffness, position, and damping. All models were developed in MATLAB to solve for natural frequencies, mode shapes, displacement transmissibility, and power spectral density (PSD) acceleration. The changes to PSD acceleration for the aspects of the model most relevant to ride comfort, i.e. sprung mass bounce and sprung mass pitch, were investigated. Results indicate that the behavior of the PSD acceleration results for sprung mass bounce and sprung mass pitch fall within expectations based on prior literature. Additionally, investigations into stiffness variation show a notable decrease in maximum PSD acceleration for sprung mass bounce with inconclusive results for sprung mass pitch. Moving the rear isolator down and away from the powertrain center of gravity (COG) results in a comparatively smaller decrease in maximum sprung mass bounce PSD acceleration, but sprung mass pitch shows a uniform decrease. Damping increases show the greatest amount of maximum PSD acceleration decrease for both sprung mass pitch and sprung mass bounce. Finally, four combinations of damping and stiffness parameters feature conflicting results for the significance of stiffness and damping contributions to reducing PSD acceleration for the sprung mass. The investigation into the above areas needs to be expanded in the future to validate results with experimental data and by investigating the full behavior changes to PSD acceleration plots, as opposed to solely inspecting PSD acceleration maxima; this will capture changes to other peaks and bandwidths that may impact qualitative and quantitative assessment of ride comfort. Additionally, the model can be augmented with a representation of specific rider interfaces such as hands, feet, and torso, along with investigations into different parameters, such as varying vehicle speed and different road input types. Such an analytical model in conjunction with experimental validation will provide a more complete understanding of the ride comfort sensitivity to the rear powertrain mounting system.

Acknowledgments

Obtaining my master's degree would not have been possible without the constant advice and support of my family. Additionally, I would like to extend my thanks to Nate Bledstein, who, as a fellow graduate student, assisted in the early stages of the modeling. Special thanks is needed for both the Mechanical Engineering Department at MSOE for constant assistance and support, and specifically Dr. Sudhir Kaul, for his guidance throughout.

Table of Contents

List of Figures

List of Tables

Nomenclature

Symbols

b = Distance from Rear Tire Contact Point to Center of Gravity

c_f = Front Suspension Equivalent Vertical Linear Damping

c_r = Rear Suspension Equivalent Vertical Linear Damping

c_{1fx} = Front Isolator Equivalent Horizontal Damping Coefficient

c_{1fy} = Front Isolator Equivalent Vertical Damping Coefficient

c_{1rx} = Rear Isolator Equivalent Horizontal Damping Coefficient

c_{1ry} = Rear Isolator Equivalent Vertical Damping Coefficient

I = Mass Moment of Inertia for Sprung Mass

k_f = Front Suspension Equivalent Vertical Stiffness Coefficient

k_{pf} = Front Tire Equivalent Stiffness Coefficient

k_{pr} = Rear Tire Equivalent Stiffness Coefficient

k_r = Rear Suspension Equivalent Vertical Stiffness Coefficient

k_{1fx} = Front Isolator Equivalent Horizontal Stiffness Coefficient

k_{1fy} = Front Isolator Equivalent Vertical Stiffness Coefficient

k_{1rx} = Rear Isolator Equivalent Horizontal Stiffness Coefficient

k_{1ry} = Rear Isolator Equivalent Vertical Stiffness Coefficient

m = Mass - Sprung Mass

m_f = Mass – Front Unsprung Mass

m_r = Mass – Rear Unsprung Mass

p = Wheelbase

x_p = Powertrain Horizontal Translation

x_r = Rear Unsprung Mass Horizontal Translation

y = Sprung Mass Vertical Translation

y_f = Front Unsprung Mass Vertical Translation – Front unsprung mass hop

y_p = Powertrain Vertical Translation

y_r = Rear Unsprung Mass Vertical Translation – Rear unsprung mass hop

γ = Powertrain Pitch

θ = Sprung Mass Pitch

Abbreviations

COG – Center of Gravity

DOF – Degree-of-Freedom

EOM – Equation of Motion

FRF – Frequency Response Function

PSD – Power Spectral Density

VDV – Vibration Dose Value

Introduction

The subject of rider comfort with respect to motorcycle dynamics is an active field of research. Existing studies in ride comfort analysis range from investigations into the influence of linear and nonlinear engine isolation versus rigidly mounted engines by Kaul [1, 2] to correlating physical road input vehicle data collection with rigid-flexible coupling simulations [3]. This project's purpose is to build upon the understanding of the in-plane dynamics of a motorcycle with an isolated powertrain. Specifically, the focus of the project is to understand the influence of the rear vibration isolation system's stiffness, position, and damping characteristics on the planar dynamics relating to ride comfort behavior of a motorcycle under random road inputs.

The report is organized as follows. A background is provided on the investigation addressed with a summary of the work carried out prior to this analysis as well as a description of important issues relating to the topic of investigation. A brief literature review then discusses how others have addressed the topic. Following the background, the methods of model development, verification, and analysis are provided in detail. Results for the eight-degree-of-freedom (DOF) model are then presented and discussed, followed by a conclusion that summarizes the work completed with details on potential continuations of research in this area.

Background

Motorcycle dynamic modeling can be divided into two broad categories: in-plane analysis and out-of-plane analysis. In-plane models are typically applied to investigate ride comfort of the vehicle with road irregularities as the primary inputs. The in-plane

models that exist today can range from simplified representations of two-wheeled vehicles to relatively more complex models for vehicles such as those with isolated powertrains [1]. Additionally, models have been developed to capture dynamics at key rider interfaces such as hands, feet, or torso to gain a better understanding of ride comfort in those areas [4]. Out-of-plane models are typically applied to investigate vehicle handling, maneuverability, and stability.

Ride comfort analysis with in-plane, or planar, models has historically been applied to target numerical and subjective requirements [4]. Such requirements are based on the intended purpose of the vehicle. For instance, a vehicle that is intended for long highway miles will likely hold ride comfort requirements in higher regard compared to a sport vehicle that is intended for achieving competitive lap times on-track [4]. Commercial manufacturers apply different techniques to mitigate ride comfort concerns, which can range from suspension optimization to mitigating shaking forces from the powertrain through balancing or through powertrain isolation from the chassis [1].

Powertrain isolation in motorcycles often involves mounting the powertrain to the frame of the vehicle through different combinations of isolators at the front and rear of the powertrain [1]. The influence of isolator stiffness, position, and damping on the road irregularity responses are important characteristics to understand for both the in-plane and out-of-plane dynamics of a motorcycle. Additionally, an independent understanding of components, such as vibration isolator planar behavior, can benefit vehicle performance trouble-shooting and full-vehicle dynamic simulation efforts [5]. For instance, multi-body dynamics models of motorcycles can be developed in existing software such as BikeSim (Mechanical Simulation) and FastBike (Dynamotion) [4]. Such

programs can be beneficial resources during the design and analysis of the vehicle. However, if an issue is present with vehicle performance, identifying the design parameters that would be beneficial to modify may be challenging with the BikeSim and FastBike programs as their use for component-level analysis is limited relative to their uses for full-vehicle dynamic analysis [1]. Similarly, general multi-body dynamics software, such as Altair MotionSolve, can be applied to represent dynamic events through established building blocks within the program [1]. However, a deeper engineering understanding of component-level behavior, beyond the provided building blocks, is often beneficial in refining the model and integrating the component-level characteristics with the system level model. This engineering understanding can be applied through additional logic imported into a general multi-body dynamics model. In the case of vibration isolator influence, the model and understanding of isolator behavior could then be applied to a broader multi-body dynamics model to better predict vehicle ride comfort [6].

Literature Review

Gonçalves and Ambrosio [6] proposed a method for flexible multibody models which represent complex bodies using general finite element methods. The model is applied for road vehicles. Multiple road profiles are used with different speeds to cover a broad set of conditions a vehicle would typically undergo during normal operation. Ride comfort ratings for the modeled vehicle are established through weighted values representing the importance of each respective vibration relative to distinct frequency ranges. The range critical for ride comfort analysis is 0 to 25 Hz, where vibrations within

this range are described as tactile and visual. This vibration range and weighting scale, based on information from ISO 2631, is then applied to key interfaces between the passenger and the vehicle: feet, hands, and torso. Vibrations higher than 25 Hz are classified as noise and are not included in the ride comfort evaluation. The weighting analyses of each frequency are then combined to produce an overall vibration dose value (VDV). The resulting model is not compared to experimental data but does demonstrate the effectiveness of a multibody model in efficiently optimizing suspension characteristics and frame stiffness for vehicle ride comfort.

A method has been established by Cossalter *et al.* [4] for evaluating the ride comfort of a motorcycle within the frequency domain. The focus of the paper is around road irregularities causing vertical displacements of the front and rear wheels, which in turn impact suspension, chassis, and rider. Additionally, the model proposed by Cossalter *et al.* [4] includes wheelbase filtering, which accounts for a delay between the contact of the front tire and the rear tire with road irregularities. Engine shaking forces and other sources of excitation are not considered in this study. The road irregularities cause vibrations through the mechanical systems of the motorcycle, resulting in accelerations that are perceived by the rider. To evaluate sprung mass vibrations resulting from the road profile, three frequency ranges are applied by Cossalter *et al.* as follows: “the quasi-static range (frequency $v < 0.5$ Hz), the ride range ($0.5 < v < 20$ Hz) and the acoustic range ($20 < v < 20\,000$ Hz)” [4]. These ranges are notably similar to those presented by Gonçalves and Ambrosio as both papers cite ISO 2631 as a primary source for understanding comfort levels relative to vibration and frequency ranges [4, 6]. The proposed model determines the PSD of the motorcycle seat acceleration over random road profiles.

Additionally, missions, or the “journeys with a forward speed that assumes different values according to a probability density function” [4] are applied to take the influence of varying vehicle speed into account in an efficient manner.

A model has been developed by Kaul [7] intended for the non-linear analysis of mechanical snubbing in elastomeric isolators. Three degrees-of-freedom are proposed for the system: lumped mass vertical translation, fore-aft translation, and pitch. This model captures the strain rate and strain amplitude dependence of the snubbing system and shows general agreement with experimentally collected load-displacement data from a test rig. The model could be applied to optimize system behavior such as transmitted forces of an isolated powertrain to a surrounding chassis or even to determine the displacement envelope of an isolated motorcycle powertrain to prevent contact with a surrounding chassis [7].

A systematic review by Rouillard and Sek [8] identifies the need to simulate random road input conditions to obtain representative results from planar dynamics models. One method to represent random road inputs is through a power spectral density (PSD) function. PSD is the measure of a given signal’s power content versus frequency. In this instance, the elevation profile of a given section of road is taken as the signal and the corresponding power. The PSD function can be approached in two ways. The first method is the collection of data on the vehicle in question in a specified vehicle operating environment under varying road undulations. These data sets can then be used to calculate a targeted PSD function. This method is often viewed as the most representative approach and allows for the PSD function to be tailored specifically to the vehicle. The

second approach involves pulling from existing PSD functions from similar vehicles and environments [8].

The model developed by Kaul [1] for an isolated powertrain motorcycle is a foundational element to the ride comfort analysis presented in this report. Kaul's eight-DOF model characterizes the planar dynamics of a motorcycle with linearly represented vibration isolation and suspension systems. A comparison is made to a rigidly mounted powertrain system to understand the influences of the isolation system under random road irregularities represented by the PSD of the road profile. Results of the study show notable changes in sprung mass pitch and for the rear unsprung mass hop for the isolated powertrain model relative to the rigid powertrain model. The study was conducted at a single speed, but the changes in sprung mass pitch and rear unsprung mass hop behavior indicate an impact on the handling of the motorcycle due to the isolation system that should be taken into consideration during the design process [1].

Methods

Model Overview

Two planar motorcycle ride comfort models have been applied for this MSE Capstone Project: a four-DOF, rigidly mounted powertrain model, and an eight-DOF isolated powertrain model. The models have been applied within MATLAB and solved for natural frequencies, mode shapes, displacement transmissibility, and PSD acceleration. For the PSD analysis, the motorcycle is being driven at a constant speed in a straight line with varying conditions of the road surface.

The four-DOF model, as seen in Figure 1, has a central sprung mass. The sprung mass is a rigid-body that combines all vehicle components above the front and rear suspension: chassis, powertrain, and rider. In the four-DOF model, the powertrain is rigidly mounted to the chassis, and therefore, it is a component of the sprung mass. Additionally, there is no distinction between the rider and the chassis, and the rider is assumed to be a perfectly rigid member of the sprung mass. However, the model could be expanded to more accurately represent rider interfaces with the vehicle by adding separate degrees of freedom to represent the hands, feet, and torso of the rider. The front unsprung mass, m_f, and the rear unsprung mass, m_r, represent the front and rear wheel assemblies, which include all components under the suspension systems: wheel, tire, brake, and axle. The front and rear suspension systems connect the sprung mass to each respective unsprung mass. As the suspension systems are comprised of two shocks or two fork legs each, these are treated as parallel systems. In turn, the contributions of each pair are represented as single equivalent spring-damper components in the model. Two points of contact represent the interfaces between the tires and road. Realistically, the tires would conform to the ground's flat surface in a distributed area known as the contact-patch, but this idealization has been made to reduce the model's complexity. Between these contact points and the unsprung masses, another set of spring-damper systems represent equivalent tire stiffness and damping. However, tire damping is generally accepted as being small relative to the front and rear suspension damping and is dependent on the excitation applied [9]. To reduce model complexity, tire damping has been ignored for the analysis performed in this study, but the model does have the capability to include tire damping for any future work in this area.

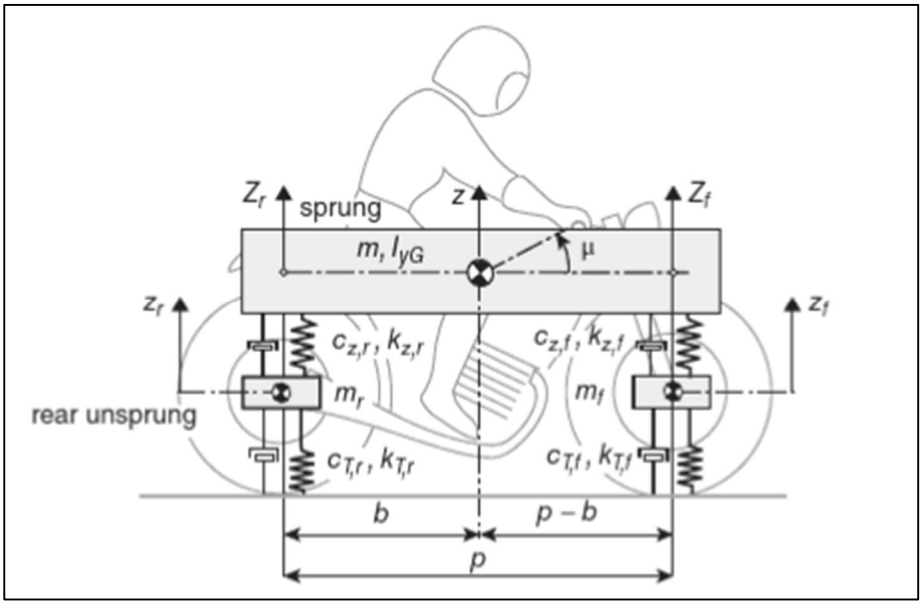

Figure 1: Four-DOF Planar Motorcycle Model [5].

The eight-DOF model, as seen in Figure 2, is similar to the four-DOF model with the primary difference being the separation of the powertrain, m_p and I_p, from the sprung mass, m and I, through two isolators at the front and two isolators at the rear of the powertrain. Similar to the front and rear suspension systems, the two pairs of isolators are treated as symmetrical components represented by their respective equivalent horizontal and vertical damping and stiffness. Since the powertrain is connected to the rear unsprung mass through a swingarm (represented by the dashed line in Figure 2), the isolation system is coupled to the rear unsprung mass.

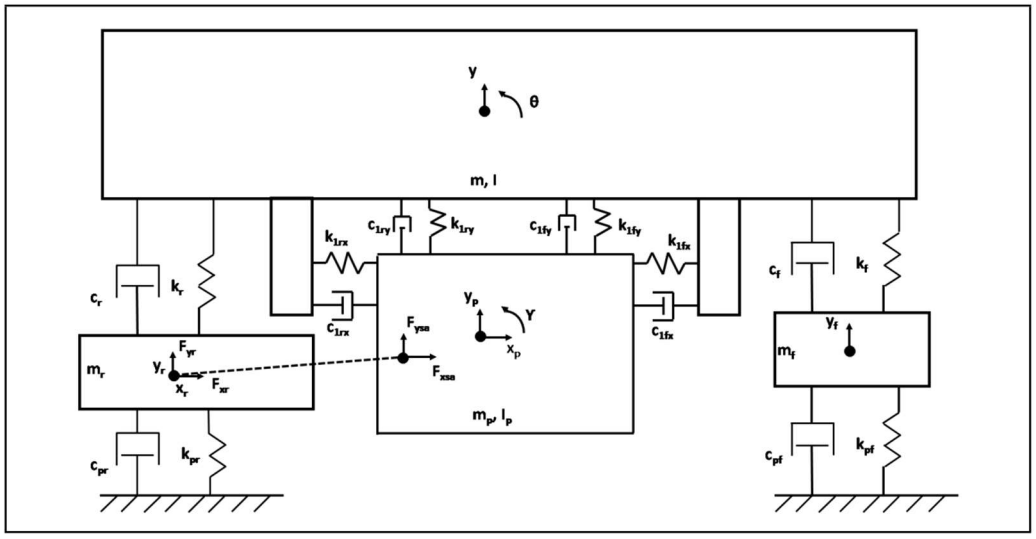

Figure 2: Eight-DOF Planar Motorcycle Model [1].

In sum, the four-DOF model has the following DOFs: sprung mass bounce (y), sprung mass pitch (θ), front unsprung mass hop (y_f), and rear unsprung mass hop (y_r). The term bounce and hop refer to the vertical displacements of the sprung and unsprung masses, respectively. The eight-DOF model expands on the initial DOFs with the following: powertrain bounce (y_p), powertrain pitch (γ_p), powertrain fore-aft (x_p), and rear unsprung mass fore-aft (x_r).

Analysis Methods

Three primary methods have been applied to investigate the two models: mode shape analysis, displacement transmissibility, and PSD acceleration. Both the four-DOF and eight-DOF models are based around equations of motion associated with each DOF that may be coupled with other DOF; these EOM form the foundation of the analysis. Both models apply the equations of motion (EOM), transmissibility equations, and PSD

acceleration as presented by Kaul [1]. The EOMs for the eight-DOF model are discussed further in this section. The dimensions of the motorcycle within the model are primarily the wheelbase, p, and the horizontal distance from the rear tire contact point to the center of gravity (COG), b. The interaction force due to swingarm stiffness between the powertrain and rear unsprung mass are represented by F_{xsa}, F_{ysa}, F_{xr}, and F_{yr}. Stiffnesses and damping parameters for the eight-DOF system are listed in Table 1.

Table 1: Stiffness and Damping Parameters for the Eight-DOF System.

Variable	Description
k_f	Front Suspension Equivalent Vertical Stiffness Coefficient
k_{pf}	Front Tire Equivalent Stiffness Coefficient
k_{pr}	Rear Tire Equivalent Stiffness Coefficient
k_r	Rear Suspension Equivalent Vertical Stiffness Coefficient
k_{1fx}	Front Isolator Equivalent Horizontal Stiffness Coefficient
k_{1fy}	Front Isolator Equivalent Vertical Stiffness Coefficient
k_{1rx}	Rear Isolator Equivalent Horizontal Stiffness Coefficient
k_{1ry}	Rear Isolator Equivalent Vertical Stiffness Coefficient
c_f	c_f = Front Suspension Equivalent Vertical Linear Damping
c_r	c_r = Rear Suspension Equivalent Vertical Linear Damping
c_{tf}	c_{tf} = Front Tire Equivalent Vertical Linear Damping
c_{tr}	c_{tr} = Rear Tire Equivalent Vertical Linear Damping
c_{1fx}	c_{1fx} = Front Isolator Horizontal Damping Coefficient
c_{1fy}	c_{1fy} = Front Isolator Vertical Damping Coefficient
c_{1rx}	c_{1rx} = Rear Isolator Horizontal Damping Coefficient
c_{1ry}	c_{1ry} = Rear Isolator Vertical Damping Coefficient

The applied system of equations derived from Kaul [1] begins with the sprung mass equations of motion, Equations (1) and (2):

$$m\ddot{y} + \left(k_f + k_r + k_{1fy} + k_{1ry}\right)y - k_f y_f - k_r y_r + \left[k_f(p - b) - k_r b + k_{1fy}x_{f1} - k_{1ry}x_{r1}\right]\theta + \left(k_{1ry}x_{r1} - k_{1f}\ x_{f1}\right)\gamma + \left(-k_{1fy} - k_{1ry}\right)y_p + \left(c_f + c_r + c_{1fy} + c_{1ry}\right)\dot{y} - c_f\dot{y}_f - c_r\dot{y}_r + \left[c_f(p - b) - c_r b + c_{1fy}x_{f1} - c_{1ry}x_{r1}\right]\dot{\theta} + \left(c_{1ry}x_{r1} - c_{1fy}x_{f1}\right)\dot{\gamma} + \left(-c_{1fy} - c_{1ry}\right)\dot{y}_p = 0, \quad (1)$$

and,

$$\mathrm{I}\ddot{\theta} + \left[k_f(p - b)^2 + k_r b^2 + k_{1fy}{x_{f1}}^2 + k_{1ry}{x_{r1}}^2\right]\theta + \left[k_f(p - b) - k_r b + k_{1fy}x_{f1} - k_{1ry}x_{r1}\right]y - k_f(p - b)y_f + k_r b y_r + (k_{1ry}x_{r1} - k_{1fy}x_{f1})y_p + (-k_{1fy}{x_{f1}}^2 - k_{1r}\ {x_{r1}}^2)\gamma + \left[c_f(p - b)^2 + c_r b^2 + c_{1fy}{x_{f1}}^2 + c_{1ry}{x_{r1}}^2\right]\dot{\theta} + \{c_f(p - b) - c_r b + c_{1fy}x_{f1} - c_{1ry}x_{r1}]\ \dot{y} - c_f(p - b)\dot{y}_f + c_r b\dot{y}_r + (c_{1ry}x_{r1} - c_{1fy}x_{f1})\dot{y}_p + \left(-c_{1fy}{x_{f1}}^2 - c_{1ry}{x_{r1}}^2\right)\dot{\gamma} = 0. \quad (2)$$

Equations (3), (4) and (5) represent the front and rear unsprung mass hop,

$$m_f\ddot{y}_f - k_f y - k_f(p - b)\theta + \left(k_f + k_{pf}\right)y_f - c_f\dot{y} - c_f(p - b)\dot{\theta} \quad + (c_f + c_{pf})\dot{y}_f = 0, \quad (3)$$

$$m_r\ddot{x}_r = F_{xr}, \quad (4)$$

$$m_r\ddot{y}_r + \left(k_{pr} + k_r\right)y_r - k_r y + k_r b\theta + \left(c_{pr} + c_r\right)\dot{y}_r - c_r\dot{y} \qquad + c_r b\dot{\theta} = F_{yr}\ , \quad (5)$$

and the powertrain fore-aft, bounce, and pitch EOMs are represented in Equations (6), (7), and (8),

$$m_p\ddot{x}_p + \left(k_{1fx} + k_{1rx}\right)x_p + \left(k_{1rx}y_{r1} - k_{1fx}y_{f1}\right)\gamma + \left(c_{1fx} + c_{1rx}\right)\dot{x}_p + \left(c_{1rx}y_{r1} - c_{1fx}y_{f1}\right)\dot{\gamma} = F_{xsa}\,, \tag{6}$$

$$m_p\ddot{y}_p + \left(k_{1fy} + k_{1ry}\right)y_p + \left(k_{1fy}x_{f1} - k_{1ry}x_{r1}\right)\gamma + \left(-k_{1fy}x_{f1} + k_{1ry}x_{r1}\right)\theta + \left(-k_{1fy} + k_{1ry}\right)y + \left(c_{1fy} + c_{1ry}\right)\dot{y}_p + \left(c_{1fy}x_{f1} - c_{1ry}x_{r1}\right)\dot{\gamma} + \left(-c_{1fy}x_{f1} + c_{1ry}x_{r1}\right)\dot{\theta} + \left(-c_{1fy} - c_{1ry}\right)\dot{y} = F_{ysa}\,, \tag{7}$$

$$\mathrm{I}_p\ddot{\gamma} + \left(k_{1fx}{y_{f1}}^2 + k_{1fy}{x_{f1}}^2 + k_{1rx}{y_{r1}}^2 + k_{1ry}{x_{r1}}^2\right)\gamma + (k_{1rx}y_{r1} - k_{1fx}y_{f1})x_p + (k_{1fy}x_{f1} - k_{1ry}x_{r1})y_p + (-k_{1fy}x_{f1} + k_{1ry}x_{r1})y + (-k_{1fy}{x_{f1}}^2 - k_{1ry}{x_{r1}}^2)\theta + \left(c_{1fx}{y_{f1}}^2 + c_{1f}\ {x_{f1}}^2 + c_{1rx}{y_{r1}}^2 + c_{1ry}{x_{r1}}^2\right)\dot{\gamma} + (c_{1rx}y_{r1} - c_{1fx}y_{f1})\dot{x}_p + (c_{1fy}x_{f1} - c_{1ry}x_{r1})\dot{y}_p + (-c_{1fy}x_{f1} + c_{1ry}x_{r1})\dot{y} + (-c_{1fy}{x_{f1}}^2 - c_{1ry}{x_{r1}}^2)\dot{\theta} = F_{xsa}y_{sa} - F_{ysa}x_{sa}. \tag{8}$$

Equations (1) through (8) constitute the foundational elements of the modal, displacement transmissibility, and PSD acceleration analyses [1].

The mode shapes have been identified to understand the coupling between the different DOFs within the system [1]. Mode shapes have been scaled to ± 1 and results corresponded to each of the DOFs. From there, coupling between degrees-of-freedom can be identified with a specific natural frequency with a mode shape magnitude within ±1. The natural modes allow an understanding of the inherent dynamic characteristics of the system and the interaction between different degrees-of-freedom [1].

Displacement transmissibility is the ratio of a DOFs output displacement (position or angle) to the system input [10]. Displacement transmissibility is a good dimensionless indicator that can be used to comprehend the results from natural frequencies and mode shapes, which can then be used to explain some of the results from the PSD acceleration plots. However, displacement transmissibility may not be a direct representation of ride comfort as it would need to be differentiated into acceleration transmissibility to draw ride comfort conclusions. This is because the accelerations perceived by the rider are the primary indicator of discomfort [4]. Therefore, displacement transmissibility has not been used to derive any ride comfort conclusions. In this model, the input was road irregularities represented by sinusoidal inputs as base excitation. Along with these inputs, a phase delay between the front and rear tire contact points has been accounted for, which is known as wheelbase filtering. Under excitation frequency, ω, displacement transmissibility, T, is derived by Equation (9),

$$\mathrm{T} = [-\omega^2 M + i\omega C + K]^{-1}[\acute{K} + i\omega\acute{C}], \tag{9}$$

where M, C, and K are the mass, damping, and stiffness matrices compiled from Equation (1) through (8) [1].

The $\acute{K}$ matrix,

$$\acute{\mathrm{K}} = [0 \quad 0 \quad k_{pf} \quad 0 \quad k_{pr} \quad 0 \quad 0 \quad 0]^T, \tag{10}$$

and $\acute{C}$ matrix,

$$\acute{C} = [0 \quad 0 \quad c_{pf} \quad 0 \quad c_{pr} \quad 0 \quad 0 \quad 0]^T, \tag{11}$$

represent the base excitation applied to determine displacement transmissibility [1].

PSD acceleration is well documented as a method for evaluating vehicle ride comfort [4]. PSD acceleration for vehicle ride comfort models represents the magnitude of acceleration for a given mode under the influence of the road profile's PSD function. The PSD function of the road profile characterizes the magnitude of surface irregularities as a function of their wavelength. For the purposes of this model, a PSD constant, S_{rr}, representing a standard road profile with good surface quality has been applied. PSD acceleration results can then be inspected in the following ways. Higher magnitudes of PSD acceleration indicate stronger vibrations for the sprung mass. Larger bandwidths indicate that the vibrations will be present across a wider range of frequencies. Significant peaks and bandwidths can then be compared to an established understanding of human sensitivity to vibrations to understand the potential impact on ride comfort. The frequency response function (FRF), represented by *H(ω),*

$$H(\omega) = -\omega^2[-\omega^2 M + i\omega C + K]^{-1}[\hat{K} + i\omega\hat{C}], \tag{12}$$

along with the $\hat{K}$ matrix,

$$\hat{K} = \begin{bmatrix} 0 & 0 & k_{pf} & 0 & 0 & 0 & 0 & 0 \\ 0 & 0 & 0 & 0 & k_{pr} & 0 & 0 & 0 \end{bmatrix}^T, \tag{13}$$

and the $\hat{C}$ matrix

$$\hat{C} = \begin{bmatrix} 0 & 0 & c_{pf} & 0 & 0 & 0 & 0 & 0 \\ 0 & 0 & 0 & 0 & c_{pr} & 0 & 0 & 0 \end{bmatrix}^T, \tag{14}$$

establish the foundation of base excitation to be used in PSD acceleration derivation [1].

A modified FRF, represented by $H^*(\omega,V)$ where V is vehicle velocity,

$$H(\omega)\begin{bmatrix}1\\ e^{-i\omega\frac{p}{V}}\end{bmatrix} = H^*(\omega, V), \tag{15}$$

is applied to incorporate wheelbase filtering due to the delay of road inputs between the front and rear tire [1].

Finally, the PSD of the road profile, characterized by $S_{rr}(\omega, V)$, was selected to be 16 x 10^{-6}, which is accepted to be representative of a good road surface [5] based on ISO classification of road surfaces. From there, the $S_{ii}(\omega, V)$ equation,

$$S_{ii}(\omega, V) = |H_i{}^*(\omega, V)|^2 S_{rr}(\omega, V), \tag{16}$$

is applied to determine acceleration PSD [1].

Human Sensitivity to Vibrations

Perceived acceleration by the rider is directly related to ride comfort [4]. A method has been established by Cossalter *et al.* [4] for evaluating the ride comfort of a motorcycle within the frequency domain. To evaluate vibrations from the road profile, three frequency ranges are detailed by Cossalter *et al.* "the quasi-static range (frequency v < 0.5 Hz), the ride range (0.5 < v < 20 Hz) and the acoustic range (20 < v < 20 000 Hz)" [4]. As stated by Cossalter *et al*., if a road surface's topography falls within the quasi-static frequency range, the vehicle can be assumed to be a static system as the frequencies are low enough to not approach system natural frequencies. Quasi-static range frequencies can be thought of as if the motorcycle is riding over gradual slopes that do not engage the motorcycle suspension systems or impact the rider in a significant manner. Ride-range frequencies, which correspond to undulations of the road surface, result in

motorcycle wheel travel and suspension travel, and they impact the chassis and the rider. The ride-range frequencies are the most critical from a rider-comfort perspective. This is because the human body is most sensitive to 1 to 8 Hz frequencies while arms and hands are most sensitive to 12 to 16 Hz frequencies. The acoustic frequency range corresponds to the roughness of a road surface. The human body is less sensitive in this range, but these frequencies can cause a perceptible level of noise [4].

Model Verification Methods

The four-DOF model was used to establish a baseline set of results that could then be compared to existing literature and to act as a checkpoint to eliminate any errors prior to increasing the complexity of the model with eight DOFs. The eight-DOF model was developed as an expansion of the original four-DOF model. To check the validity of the eight-DOF model, the isolator stiffnesses around the powertrain were set to extremely high values. This was done to approach a rigid connection between the powertrain and sprung mass, and therefore approach the behavior seen in the four-DOF model results. The effort was successful, therefore validating the eight-DOF model.

Analysis Overview

Following an initial analysis of the eight-DOF model, the influence of the rear isolator's characteristics was investigated in the following ways: stiffness variation, position variation, damping variation, and with different combinations of stiffness and damping. The specific inputs used for each investigation are presented in the next section.

Results and Discussion

This section presents the results obtained from all the simulation models used for this study. Some of the trends resulting from the change of rear isolator parameters are also presented and discussed in this section.

For the results of the nominal eight-DOF model, all the input parameters can be seen in Table 2. Input parameters were selected to be realistic such that they could be reproduced in an experimental set-up. For instance, the vehicle speed was set to 17 m/s (or approximately 38 mph). As the vehicle speed plays a direct role in the vehicle's rate of interaction with the road inputs, adjusting this value would result in different behavior and should be considered as a future area of investigation.

Table 2: Nominal Eight-DOF Model Inputs.

Variable	Value
v = Vehicle Steady State Speed	17 [m/s], 38 [mph]
p = Wheelbase	1.4 [m]
b = Distance from Rear Tire Contact Point to Center of Gravity	0.7 [m]
m = Mass - Sprung Mass *	200 [kg]
mp = Mass – Powertrain	125 [kg]
I = Mass Moment of Inertia for Sprung Mass *	38 [kgm2]
Ip= Mass Moment of Inertia for Powertrain	8 [kgm2]
m_f = Mass – Front Unsprung Mass	15 [kg]
m_r = Mass – Rear Unsprung Mass	18 [kg]
k_f = Front Suspension Equivalent Vertical Stiffness	15 [kNm]
k_r = Rear Suspension Equivalent Vertical Stiffness	24 [kNm]
k_{1fx} = Front Isolator Horizontal Stiffness Coefficient	*250 [kN/m]*
k_{1fy} = Front Isolator Vertical Stiffness Coefficient	*250 [kN/m]*
k_{1rx} = Rear Isolator Horizontal Stiffness Coefficient	*250 [kN/m]*
k_{1ry} = Rear Isolator Vertical Stiffness Coefficient	*250 [kN/m]*
k_{pf} = Front Tire Stiffness	180 [kN/m]
k_{pr} = Rear Tire Stiffness	180 [kN/m]
c_f = Front Suspension Equivalent Vertical Linear Damping	900 [Ns/m]
c_r = Rear Suspension Equivalent Vertical Linear Damping	900 [Ns/m]
c_{tf} = Front Tire Equivalent Vertical Linear Damping	0 [Ns/m]
c_{tr} = Rear Tire Equivalent Vertical Linear Damping	0 [Ns/m]
c_{1fx} = Front Isolator Horizontal Damping Coefficient	900 [Ns/m]
c_{1fy} = Front Isolator Vertical Damping Coefficient	900 [Ns/m]
c_{1rx} = Rear Isolator Horizontal Damping Coefficient	900 [Ns/m]
c_{1ry} = Rear Isolator Vertical Damping Coefficient	900 [Ns/m]
x_r = Rear Isolator Horizontal Position	0.320 [m]
y_r = Rear Isolator Vertical Position	0.055 [m]
x_f = Rear Isolator Horizontal Position	0.325 [m]
y_f = Rear Isolator Vertical Position	0.020 [m]

Modal Results

With nominal inputs, the corresponding modes of the eight-DOF system can be seen in Figure 3. From these results, key relationships between degrees-of-freedom of the system pertaining to the natural modes can be identified. For the natural mode at 1.59 Hz, the sprung mass bounce is directly coupled with powertrain bounce along with some limited coupling with both sprung mass pitch and powertrain pitch. At 3.14 Hz, sprung mass pitch is coupled with powertrain pitch. The natural frequency at 9.40 Hz corresponds to the fore-aft mode of the rear unsprung mass that is coupled with the fore-aft mode of the powertrain fore-aft along with minimal coupling with both sprung mass and powertrain pitch. The natural frequency at 12.9 Hz pertains to powertrain bounce that is coupled to sprung mass bounce with minor coupling seen with the rear unsprung mass hop and powertrain pitch. The rear and front unsprung mass hops have natural frequencies at 16.9 Hz and 18.2 Hz, respectively, with little to no coupling with other degrees-of-freedom. Finally, the rear unsprung mass fore-aft mode has a natural frequency of 621 Hz with minimal coupling with the powertrain fore-aft motion. Based on the natural frequencies and their respective mode shapes, some insight is obtained into the characteristics of the PSD acceleration plots, such as the peaks associated with specific frequencies.

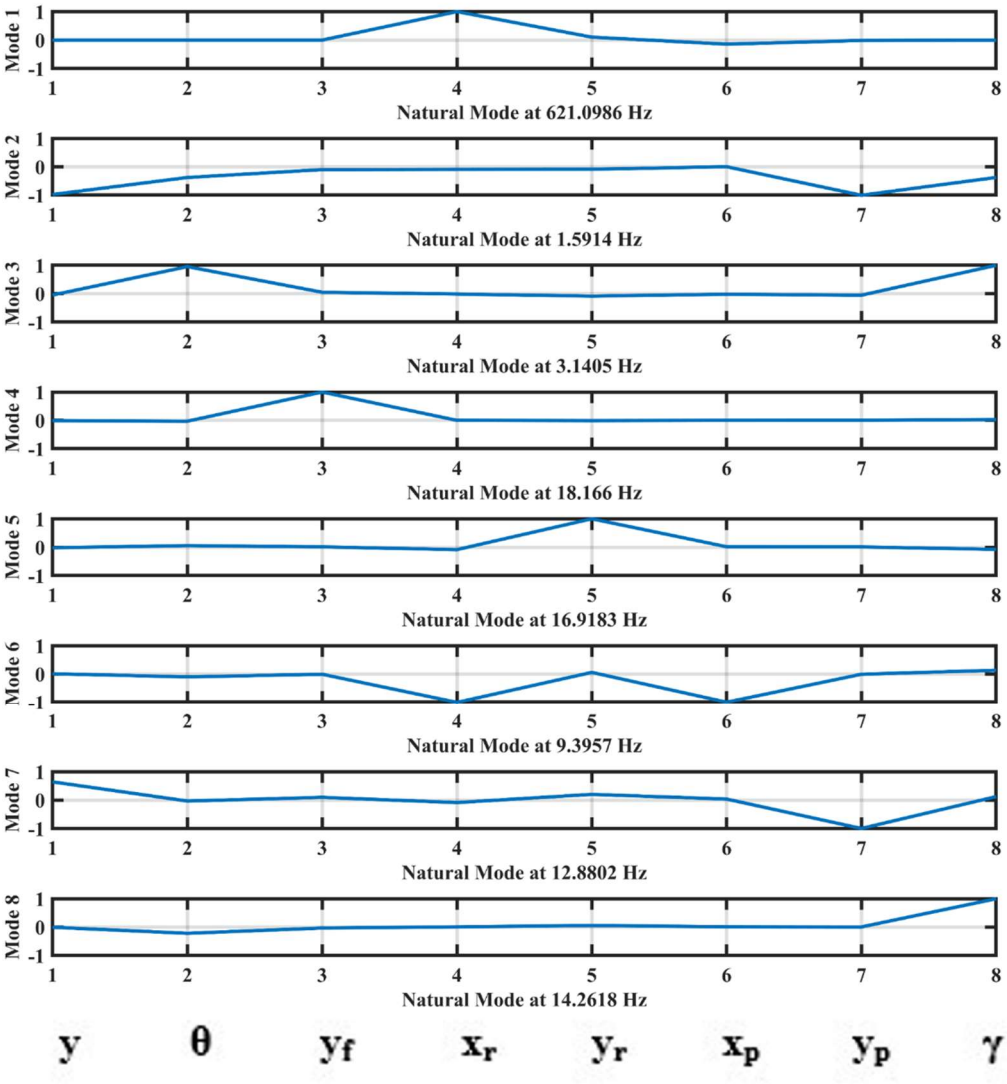

Figure 3: Eight-DOF Mode Shapes with Nominal Stiffness Values.

Displacement Transmissibility

Displacement transmissibility has also been identified for the nominal input values, but as displacement transmissibility does not directly pertain to rider comfort analysis, all results are included in the Appendix B. Acceleration transmissibility may be

used in some cases to evaluate ride comfort and compared with PSD in order to quantitatively assess a rider's exposure over specific ranges of frequency for different parts of a rider's body [4].

PSD Acceleration Nominal Inputs

The eight-DOF model with nominal inputs resulted in natural frequencies and mode shapes that fell within expectations as the scale of the mode shapes and behavior aligned with prior literature [1]. As the focus of the research is on ride comfort, the sprung mass bounce and sprung mass pitch remain the primary topic of discussion due to their significance. As seen in Figure 4, the sprung mass bounce shows the same number of peaks as the results from the four-DOF model. However, the four-DOF model does not represent separate rigid bodies for sprung mass and powertrain since the powertrain is rigidly mounted. An initial peak is seen near the 1.59 Hz natural frequency for sprung mass bounce. This peak feature a sharp magnitude with relatively small bandwidth. With this peak falling inside the ride-range frequency band, rider comfort is expected to be directly affected. The second peak, with a significantly larger amplitude and bandwidth, falls just within the ride range frequency. This peak lands at 13.7 Hz, which is likely due to the powertrain bounce coupled with the sprung mass at a natural frequency of 12.9 Hz; this mode exhibits strong coupling with pitch of the powertrain and sprung mass at a natural frequency of 14.3 Hz. However, as frequencies fall closer to the limits of the ride-range band, discomfort drops off quickly [4]. As discomfort levels are subjective, an experimental verification of the vehicle under these conditions would be required to identify whether or not the first or second peak is the primary concern for ride comfort.

The third and fourth peaks fall just outside the ride-range frequency bands with peaks at 21.6 Hz and 35.2 Hz and would not have any impact on ride comfort.

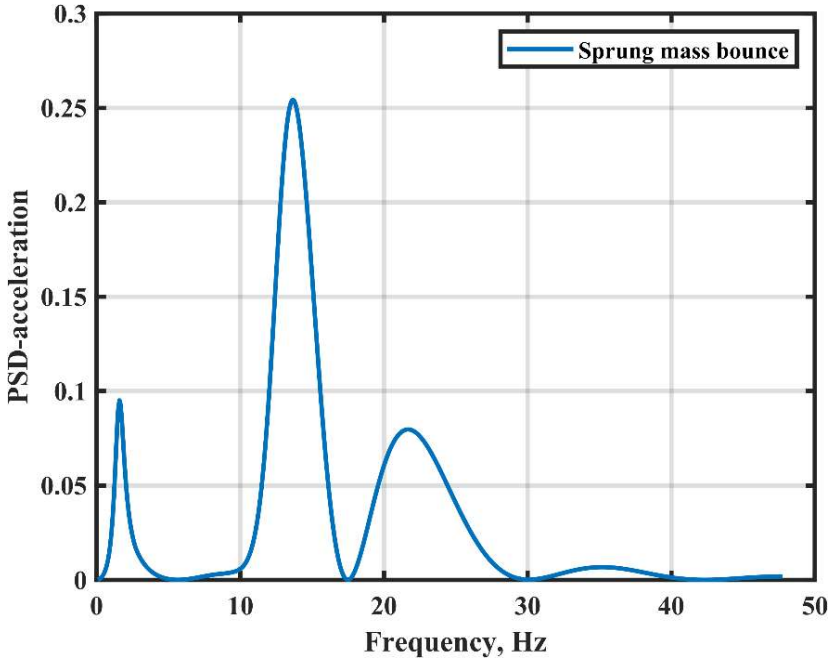

Figure 4: PSD Acceleration for Sprung Mass Bounce under Nominal Inputs.

Sprung mass pitch PSD acceleration results can be seen in Figure 5. Notably, more complex behavior can be observed; this is likely due to the interplay between the bounce and pitch of the sprung mass and powertrain and the delayed inputs at the front and rear tire contact points due to wheelbase filtering. These are larger bandwidths relative to the sprung mass bounce PSD results. However, as bounce (vertical acceleration) and pitch (angular acceleration) represent distinct types of movement, a direct comparison cannot be made between the two. Also, significant coupling between sprung mass pitch and sprung mass bounce makes it challenging to specifically attribute

the PSD to one of the two kinds of motion. Distinct behavior at 1.8 Hz, 10.8 Hz, and 14.2 Hz trends with the natural frequencies and coupling between sprung mass and powertrain bounce: 1.59 Hz sprung mass and powertrain bounce mode, 12.9 Hz sprung mass bounce and powertrain bounce mode, and 14.3 Hz powertrain pitch mode. The relatively large bandwidth between approximately 5 and 16 Hz has a relatively high magnitude within the ride-range frequency band, which corresponds to notable significance for ride comfort across a wide frequency range.

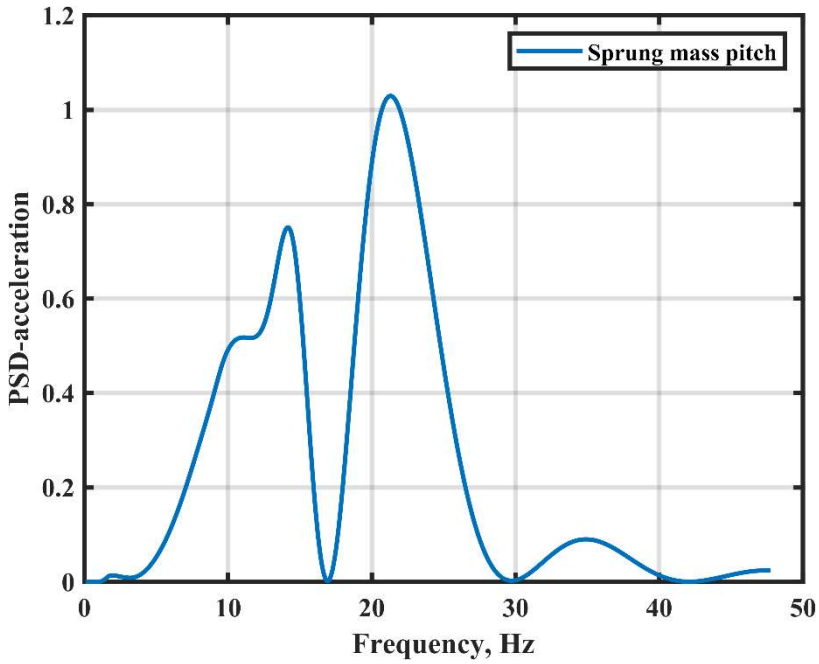

Figure 5: PSD Acceleration for Sprung Mass Pitch under Nominal Inputs.

To further investigate the contributions and impacts of rear vibration isolator parameters, stiffness, position, damping, and combinations of stiffness and damping have

been evaluated. All other input values listed in Table 2 have not been changed for all analyses reported in this section.

Stiffness Variation

The stiffness variation inputs can be seen in Table 3, which represent values plus and minus 30% of the nominal value at 10% increments.

Table 3: Rear Isolator Stiffness Variation Inputs.

Iteration	Rear Isolator Vertical Stiffness (kN/m)	Rear Isolator Horizontal Stiffness (kN/m)
1	175	175
2	200	200
3	225	225
4	250	250
5	275	275
6	300	300
7	325	325

As seen in Figure 6, the maximum PSD acceleration for sprung mass bounce starts with a small initial increase between 175 and 200 N/mm and is followed by a gradual decrease with increasing stiffness. The magnitudes decreased by 57.6% with a total change of -1.04 $(m/s^2)^2$ /Hz from the peak value. This drop is significant and indicates an improvement in ride comfort.

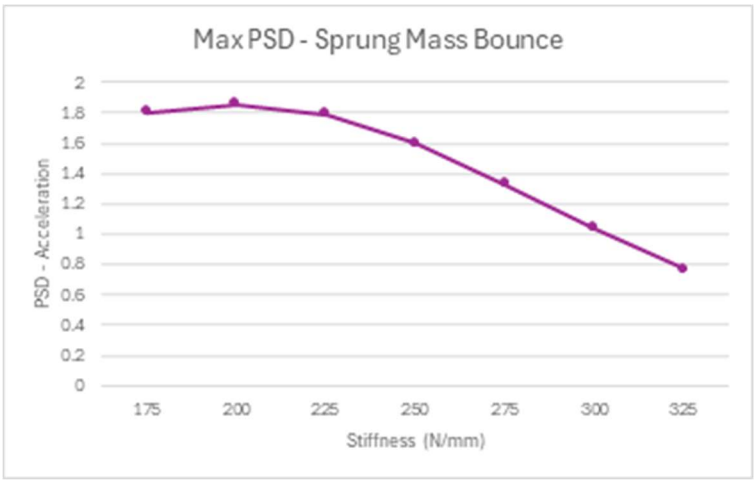

Figure 6: Stiffness Variation PSD Acceleration Maximums for Sprung Mass Bounce.

The maximum PSD acceleration stiffness variation results for sprung mass pitch can be seen in Figure 7. The resulting behavior has no discernible trend. The sudden decrease from 175 to 200 N/mm may indicate a change in the corresponding natural frequency at which the maximum PSD acceleration value occurs due to a change in the vehicle response as the pitch modes are complexly intertwined with other degrees-of-freedom of the system. A deeper investigation and comparison of the full PSD acceleration profile for all input values would be required to draw a clear conclusion. However, the investigation into the full PSD acceleration plots for all iterations was not in project scope and will need to be continued as part of any ongoing efforts.

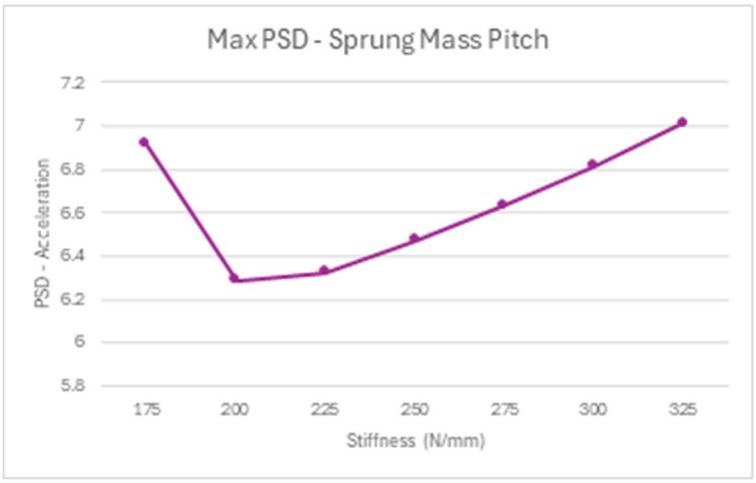

Figure 7: Stiffness Variation PSD Acceleration Maximums for Sprung Mass Pitch.

Position Variation

Rear vibration isolator position variation inputs can be seen in Table 4. The position variation inputs represent values plus and minus 30% of the nominal value at 10% increments. Position of the rear mount is relative to the center of mass of the powertrain.

Table 4: Rear Isolator Position Variation Inputs.

Position Iteration	Rear Isolator Vertical Position (m)	Rear Isolator Horizontal Position (m)
1	0.0385	0.224
2	0.044	0.256
3	0.0495	0.288
4	0.055	0.32
5	0.0605	0.352
6	0.066	0.384
7	0.0715	0.416

The sprung mass bounce's maximum PSD acceleration values show a reasonable impact with a total magnitude change of -0.6662 $(m/s^2)^2$ /Hz and a 37.9% decrease across the iterations as seen in Figure 8. There is an initial increase between iteration 1 and 2, followed by a gradual decrease that appears to taper out as the position moves farther down and away from the powertrain COG. The model maintains constant swingarm stiffness throughout the iterations for rear vibration isolator position, regardless of the varying length between the rear unsprung mass and powertrain. The influence of rear isolator position on PSD acceleration for the sprung mass bounce is apparent, but difficult to draw any explicit conclusions from.

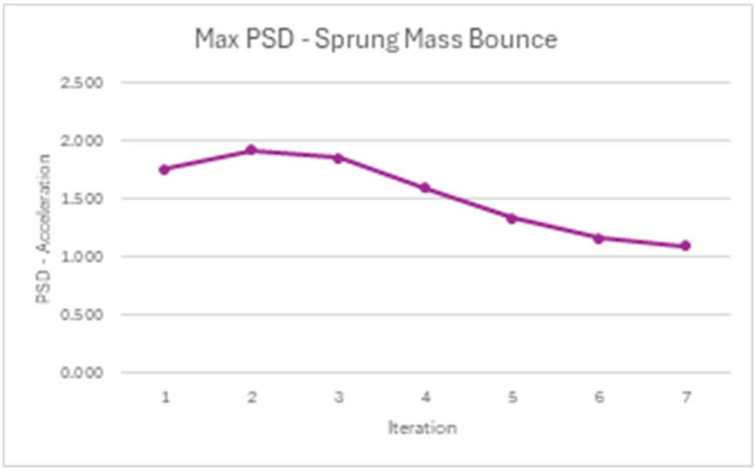

Figure 8: Position Variation PSD Acceleration Maximums for Sprung Mass Bounce.

The sprung mass bounce's maximum PSD acceleration values also exhibit a significant influence due to the change in isolator position, exhibiting a total magnitude change of -4.96 $(m/s^2)^2$ /Hz and a 42.7% decrease across the iterations as seen in Figure 9.

Notably, it appears that there is a limit to how Pitch PSD acceleration can decrease relative to moving the rear isolator down and away from the powertrain COG.

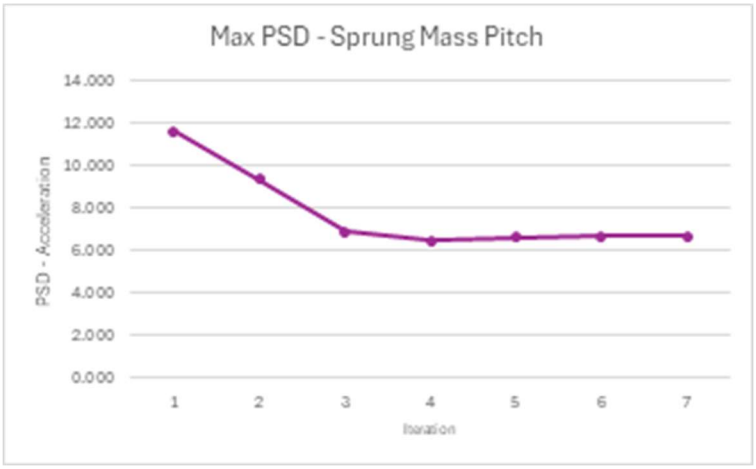

Figure 9: Position Variation PSD Acceleration Maximums for Sprung Mass Pitch.

With the understanding that an investigation of the complete PSD acceleration plots across all iterations is required to confidently draw a conclusion about a discernible trend, the apparent takeaway is that the ride comfort improves as the rear vibration isolator position moves farther down and away from the powertrain COG.

Damping Variation

The rear isolator damping variation inputs can be seen in Table 5, which represent values plus and minus 30% of the nominal value at 10% increments.

Table 5: Rear Isolator Damping Variation Inputs.

Iteration	Rear Isolator Vertical Damping (Ns/m)	Rear Isolator Horizontal Damping (Ns/m)
1	630	630
2	720	720
3	810	810
4	900	900
5	990	990
6	1080	1080
7	1170	1170

The maximum PSD acceleration of sprung mass bounce shows a significant decrease with an increase in damping, with a total magnitude change of -1.62 $(m/s^2)^2$ /Hz and a 44.9% decrease across the iterations as seen in Figure 10. As detailed by Rao [11], damping is generally expected to be the most significant contributor since increased damping is directly proportional to additional energy dissipation within the system. This, in turn, produces a clear trend of PSD acceleration magnitudes decreasing as rear isolator damping increases. The total change of the PSD acceleration of sprung mass bounce is relatively higher for damping (-1.62) as compared to stiffness (-1.04) and position (-0.662) variation.

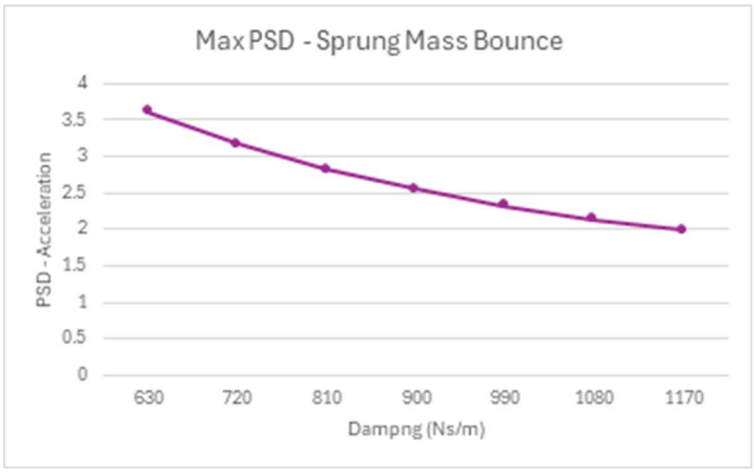

Figure 10: Damping Variation PSD Acceleration Maximums for Sprung Mass Bounce.

The maximum PSD acceleration for sprung mass bounce also exhibits a significant and consistent decrease as damping increases, with a total magnitude change of -5.05 $(m/s^2)^2$ /Hz and a 31.2% decrease across the variations as seen in Figure 11.

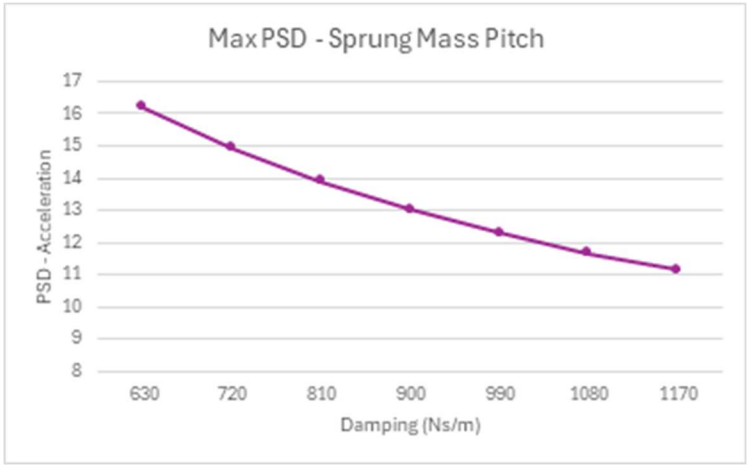

Figure 11: Damping Variation PSD Acceleration Maximums for Sprung Mass Pitch.

Damping and Stiffness Combinations

Rear vibration isolator damping and stiffness combination inputs can be seen in Table 6. The maximum and minimum values for stiffness and damping iterations seen in Table 3 and Table 5, respectively, have been simulated in four combinations.

Table 6: Rear Isolator Damping and Stiffness Combination Inputs.

Iteration	Rear Isolator Vertical & Horizontal Damping (Ns/m)	Rear Isolator Vertical & Horizontal Stiffness (kN/m)
1	1170	325
2	630	325
3	1170	175
4	630	175

For the sprung mass bounce maximum PSD acceleration values, the contributions of stiffness and damping align with expectations and may have a small dependence on one another. As seen in Figure 12, there is a 43.8% increase in magnitude between iterations 1 and 2 as damping decreases while stiffness is constant at 325 kN/m. Iterations 3 and 4 feature a 66.1% increase in magnitude when stiffness is constant at 175 kN/m. As damping decreases, the PSD acceleration peaks increase, as expected. Notably, at a lower stiffness value, the decrease in damping has a more significant effect. This could imply that for lower stiffness rear isolators, damping variation may have a greater effect on PSD acceleration magnitudes for the specific system analyzed in this study.

There is a 114% increase between iterations 1 and 3 and a 148% increase between iterations 2 and 4. It appears that, under these conditions, a stiffness decrease results in a more significant change to the PSD acceleration maximum. Additional investigation

would be needed to investigate whether or not the significant increase in PSD acceleration response for the lower stiffness input values is due to a change in the natural frequencies resulting in greater excitation at the particular velocity of the motorcycle used for this analysis.

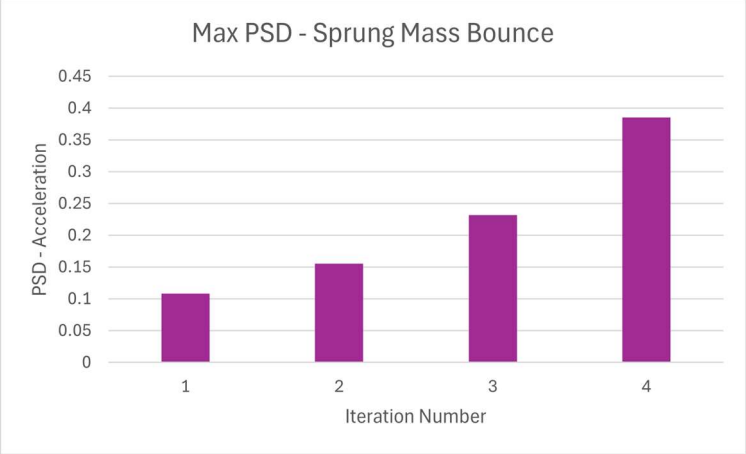

Figure 12: Damping and Stiffness Combination PSD Acceleration Maximums for Sprung Mass Bounce.

For the sprung mass pitch maximum PSD acceleration values, there is a 9.81% increase in magnitude between iterations 1 and 2 as damping decreases while stiffness is constant at 325 kN/m as seen in Figure 13. Iterations 3 and 4 feature a 32.9% increase in magnitude as damping decreases when stiffness is constant at 175 kN/m. Decreases in damping still result in lower PSD acceleration magnitudes for the sprung mass pitch. However, changes in stiffness result in inconsistent behavior for sprung mass pitch as there is a 7.44% decrease between iterations 1 and 3 and a 12.1% increase between iterations 2 and 4.

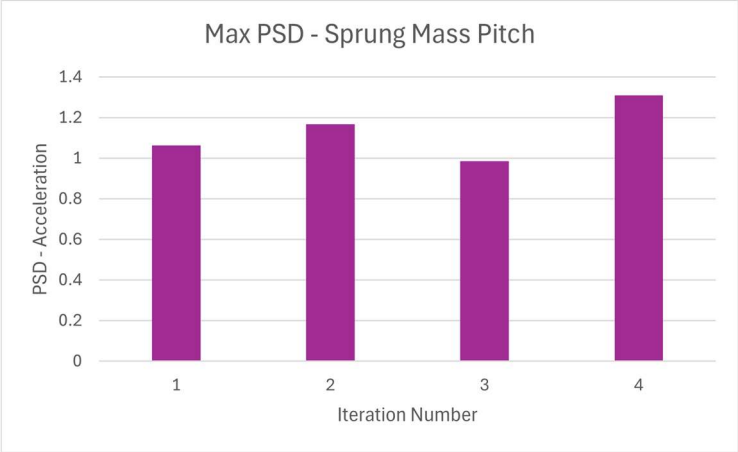

Figure 13: Damping and Position Combination PSD Acceleration Maximums for Sprung Mass Pitch.

Conclusions and Recommendations

Methods Summary

The analysis performed for this study was conducted with two planar motorcycle ride comfort models. A rigidly-mounted-powertrain four-DOF model was used to establish a baseline set of results, which can be directly compared with existing literature. An isolated-powertrain eight-DOF model was then been used to investigate the rear isolator stiffness, position, and damping influences on motorcycle ride comfort after first comparing model behavior to the four-DOF results with approximately rigid isolator stiffness parameters. Both models were developed in MATLAB and solved for natural frequencies, mode shapes, displacement transmissibility, and PSD acceleration of the motorcycle under constant speed and straight-running conditions. A review of human sensitivity to vibrations is briefly discussed with three distinct frequency ranges that are generally used for ride comfort analysis: quasi-static, ride-range, and acoustic. All ride

comfort analysis has subsequently been focused on PSD acceleration of the sprung mass within the ride-range frequency of 1 to 20 Hz.

Conclusions

The primary focus of the analysis in this MSE Capstone Project was on sprung mass bounce and sprung mass pitch as these two degrees-of-freedom are most related to the evaluation of ride comfort. Results from modal analysis identified significant coupling between bounce and pitch of the sprung mass in conjunction with the motion of the powertrain. The coupling between sprung mass bounce and sprung mass pitch can be seen to influence displacement transmissibility and PSD acceleration results for the sprung mass and the powertrain.

Nominal parameter results for the PSD acceleration of the sprung mass fell within expected ranges based on existing literature. The results for PSD acceleration also identified key areas for ride comfort analysis. Two primary peaks of PSD acceleration were present within the ride-range frequencies at 1.59 Hz and 13.7 Hz. The peak at 13.7 Hz was greater than the peak at 1.59 Hz and had a notably higher bandwidth. However, this peak approached the boundary of the ride-range frequency band, which is where the levels of discomfort begin to significantly drop off. Because of the subjective nature of ride comfort, along with the significant influence of vehicle speed and the nature of the road surface, experimental evaluation of the vehicle would be needed to validate whether or not the 13.7 Hz frequency is the greatest area of concern for ride comfort for the sprung mass bounce DOF. Sprung mass pitch is seen to be significant within the ride-

range frequency band as well with a bandwidth spanning from 5 Hz to 16 Hz and a stair-step behavior up to the maximum peak at 14.2 Hz. Notably, the magnitude of PSD acceleration for sprung mass pitch is higher than that of bounce. However, no direct comparison should be made between the bounce and pitch modes as they represent distinct types of movement and are inherently coupled.

Stiffness variation results indicated a significant and gradual decrease in the maximum PSD acceleration for sprung mass bounce as stiffness of the rear isolator increased. The results for sprung mass pitch are inconclusive with no discernible trend as there are inconsistencies between the first few stiffness iterations. This may be due to changes in corresponding natural frequencies as the isolator stiffness changes.

Position variation also exhibits a notable decrease in sprung mass bounce maximum PSD acceleration as the position of the rear isolator moves down and away from the powertrain COG. However, this change is smaller than the decrease with stiffness variation. The sprung mass pitch also behaves in a more consistent manner as the maximum PSD acceleration values have an initial steep decrease before leveling out, instead of the inconsistency seen between the first few stiffness iterations.

Damping variation exhibits a strong influence on the maximum PSD acceleration values for both the sprung mass bounce and pitch modes as compared to the stiffness and position variations. Additionally, both bounce and pitch modes decrease in a consistent manner. The significance of damping when designing for ride comfort is clear as damping is directly proportional to additional energy dissipation within the system. However, modifying isolator damping on a motorcycle is challenging due to the limits of

a passive isolator's hysteretic damping behavior as well as space limitations on the vehicle.

Of the four combinations of damping and stiffness parameters investigated, sprung mass bounce saw increases in PSD acceleration maximums as stiffness decreased as well as when damping decreased. Notably, the percent difference of PSD acceleration maximums between the two stiffness values is greater than the percent difference between the two damping values, which does not align with the previous results where damping changes had a more significant influence on PSD acceleration maximums. However, the influence of stiffness on the natural frequencies of the system may be significant and requires further investigation.

Across the four combinations applied, the sprung mass pitch exhibits inconsistent behavior between the minimum and maximum stiffness values. The combination with the lower damping saw an increase in PSD acceleration maximums as stiffness decreased. However, for the combination with the higher damping, there is a decrease in PSD acceleration maximums. The direct influence of stiffness changes on the natural frequencies of the system requires further investigation. Additionally, the pitch mode features complex coupling with the other pitch and bounce modes of the model, which make discerning behavioral trends difficult.

Limitations

The primary limitation of the analysis conducted in this study is the method of evaluating stiffness, position, and damping variations along with the combinations of

minimum and maximum stiffness and damping parameters. The maximum PSD acceleration values associated with the parameter iterations only paint a partial picture of the ride comfort behavior. An additional investigation into the full PSD acceleration plots for all iterations applied is necessary to understand the following: changes in natural frequencies, the locations of the peak PSD acceleration values relative to the ride-range frequency band, the changes to the peak bandwidths, and changes in other peaks within the resulting plots may be important in a ride comfort evaluation but fall below the overall plot maximum.

Future Research

The findings associated with this MSE Capstone Project suggest a number of possible research paths. Next steps would require validating the model with physical testing of a vehicle in straight-running conditions over a known PSD surface either in a controlled laboratory setting or on a test track. The model could be expanded to specifically target key rider interfaces with separate degrees of freedom used to represent the hands, feet, and torso of the rider. An investigation could be made into acceleration-transmissibility to augment the results of displacement transmissibility. Other parameter variations could also be investigated within the model, such as other road profiles, vehicle speeds, and different excitation sources. Finally, the most important next step would be investigating the full PSD acceleration plot for all parameter variations applied to understand the complete picture of ride comfort under varying conditions.

References

[1] Kaul, Sudhir 2020. "Influence of a Vibration Isolation System on Planar Dynamics of a Motorcycle," *International Journal of Acoustics and Vibration* Vol. 25, pp. 96-103. https://doi.org/10.20855/ijav.2020.25.11603

[2] Kaul, Sudhir 2020. "Planar Dynamics of a Motorcycle: Influence of Vibration Isolation System Nonlinearity," *International Journal of Acoustics and Vibration* Vol. 25, pp. 597-608. https://doi.org/10.20855/ijav.2020.25.41733

[3] Xihong, Zou, Shi, Quan, and Xiongxiong, Zhang. 2010, "Simulation and Verification on Motorcycle Ride Comfort under Pulse Road," *Trans Tech Publications* Vol 29-32, pp. 2544-2548. https://doi.org/10.4028/www.scientific.net/amm.29-32.2544

[4] Cossalter, Vittore, Alberto Doria, Stefano Garbin and Roberto Lot. 2006. "Frequency-Domain Method for Evaluating the Ride Comfort of a Motorcycle," *Vehicle System Dynamics*. Vol. 44, pp. 339-355. https://doi.org/10.1080/00423110500420712

[5] Cossalter, Vittore. 2006. *Motorcycle Dynamics.* 2nd Edition. Morrisville, NC, USA: Lulu

[6] Goncalves, J. P. C. and J. A. C. Ambrosio. 2003. "Optimization of Vehicle Suspension Systems for Improved Comfort of Road Vehicles Using Flexible Multibody Dynamics," *Nonlinear Dynamics*. Vol. 34, pp. 113-131. https://doi.org/10.1023/b:nody.0000014555.46533.82

[7] Kaul, Sudhir 2011. "Multi-degree-of-freedom modeling of mechanical snubbing systems," *Journal of Vibroengineering* Vol. 13, pp. 195-211. https://doi.org/10.1115/detc2011-47144

[8] Rouillard, Vincent and Sek, Michael 2012. "Creating Transport Vibration Simulation Profiles from Vehicle and Road Characteristics," *Packaging Technology and Science*. Vol. 26, pp. 82-95. https://doi.org/10.1002/pts.1967

[9] Acosta, Enrique Carabias, Juan J. Castillo Aguilar, Juan A. Cabrera Carrillo, Juan M. Velasco Garcia, Javier Perez Fernandez, and Manual G. Alcazar Vargas. 2020. "Modeling of Tire Vertical Behavior Using a Test Bench," *IEEE Access*. Vol. 8, pp. 106531-106541. https://doi.org/10.1109/access.2020.3000533

[10] Inman, Daniel J. 2006. *Vibration with Control*. West Sussex, England: John Wiley & Sons, Ltd

[11] Rao, Singiresu S. 2017. *Mechanical Vibrations*. Hoboken, NJ: Pearson Education Inc.

Appendix A. Four-DOF Nominal Results

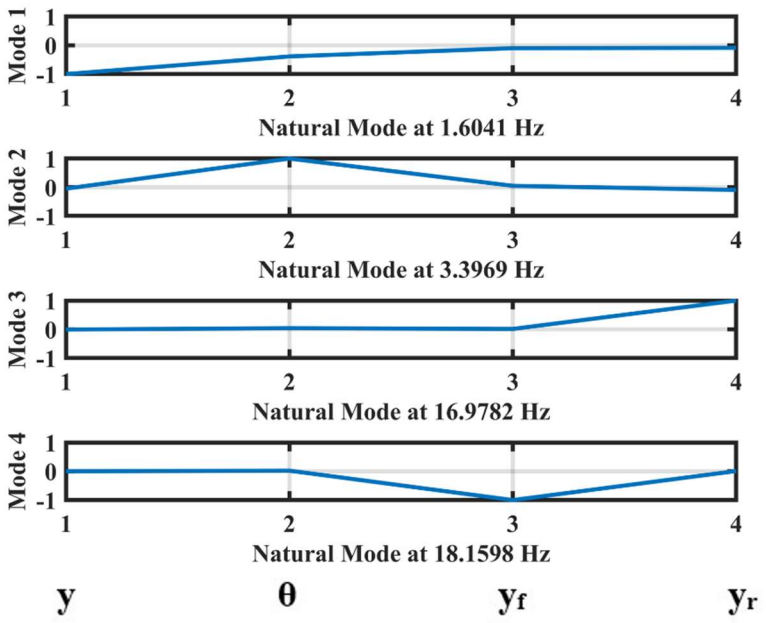

Figure A1: Four-DOF Mode Shapes.

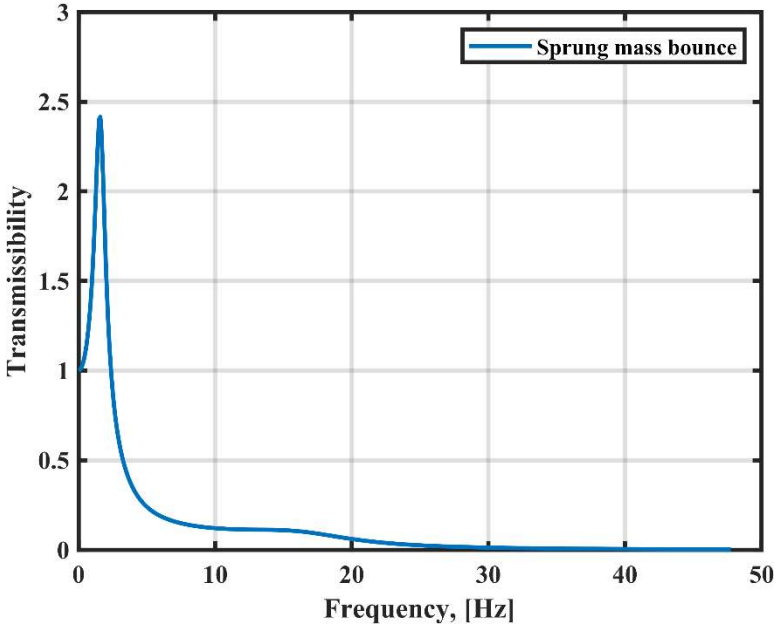

Figure A2: Four-DOF Sprung Mass Bounce Transmissibility.

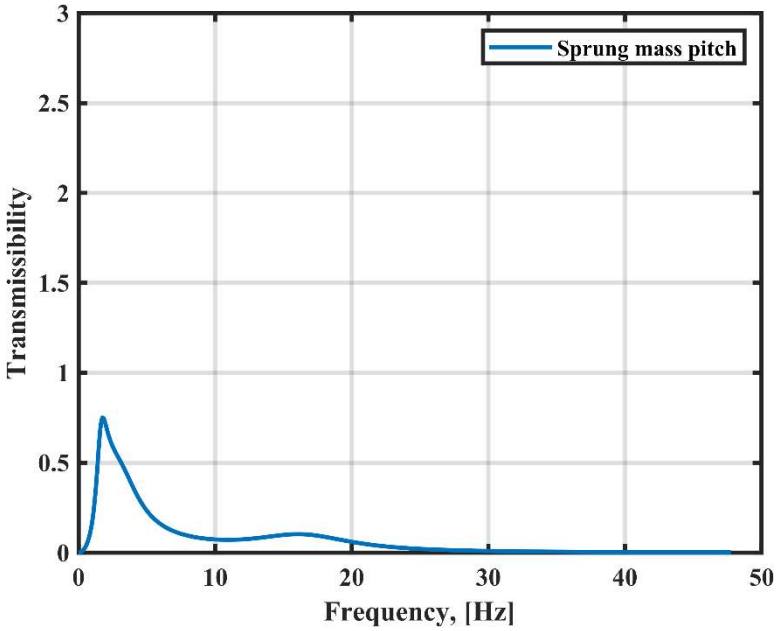

Figure A3: Four-DOF Sprung Mass Pitch Transmissibility.

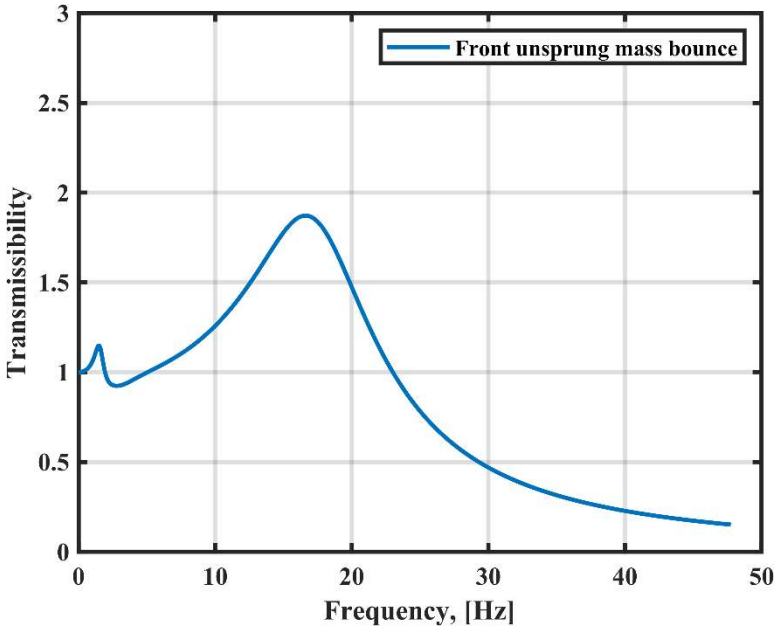

Figure A4: Four-DOF Front Unsprung Mass Hop Transmissibility.

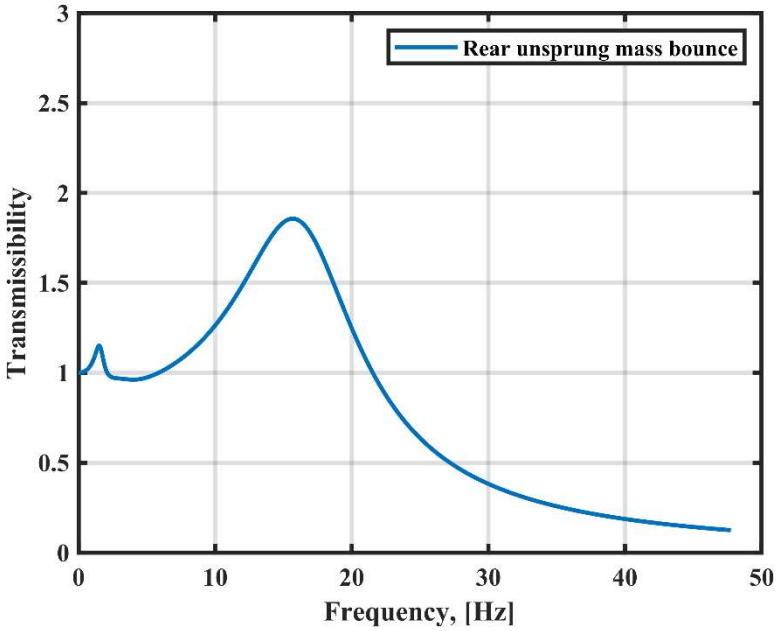

Figure A5: Four-DOF Rear Unsprung Mass Hop Transmissibility.

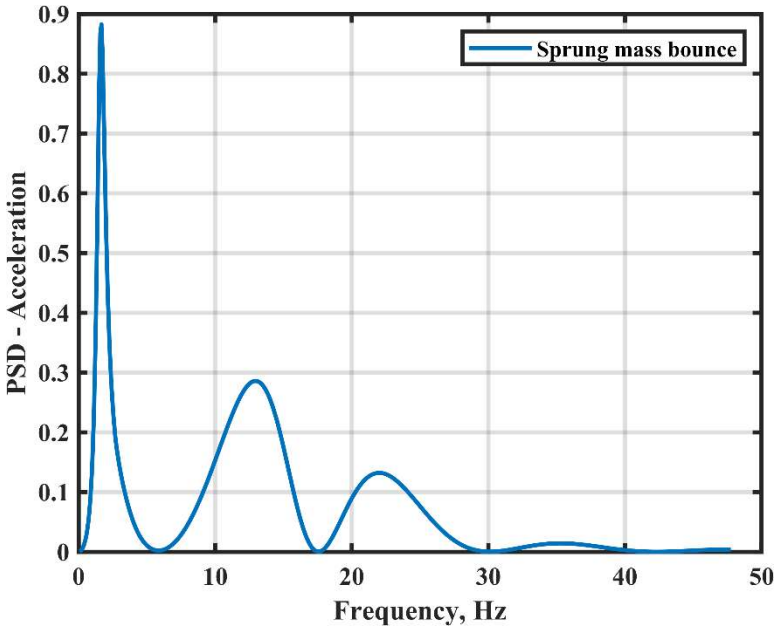

Figure A6: Four-DOF Sprung Mass Bounce PSD.

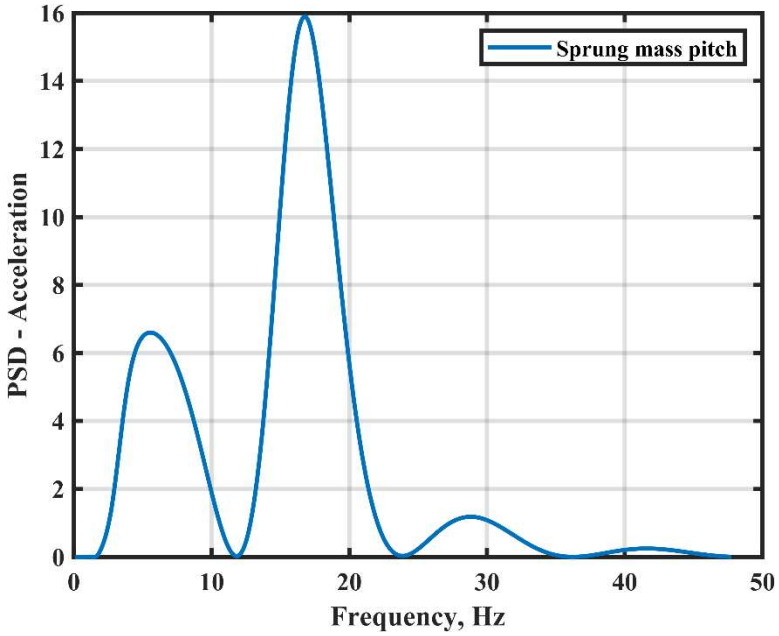

Figure A7: Four-DOF Sprung Mass Pitch PSD.

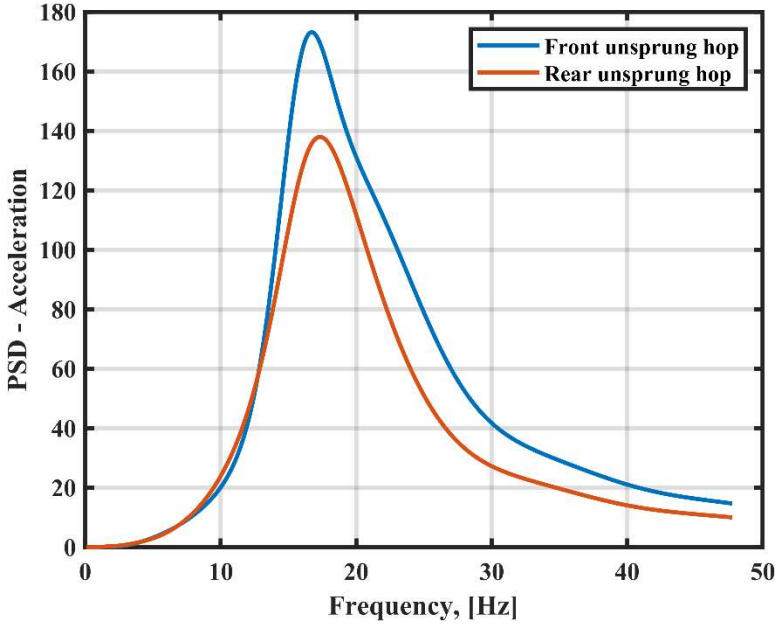

Figure A8: Four-DOF Front and Rear Unsprung Mass Hop PSD.

Appendix B. Eight-DOF Nominal Results

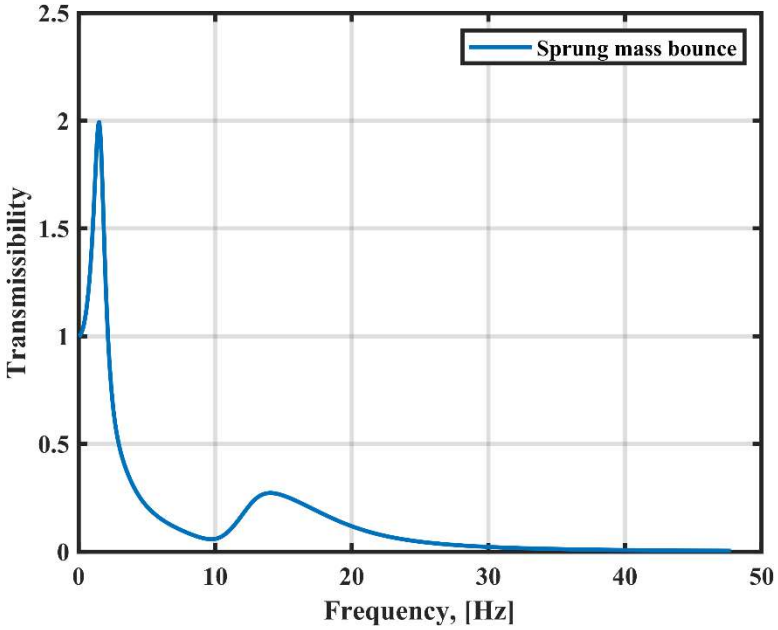

Figure B1: Eight-DOF Sprung Mass Bounce Transmissibility.

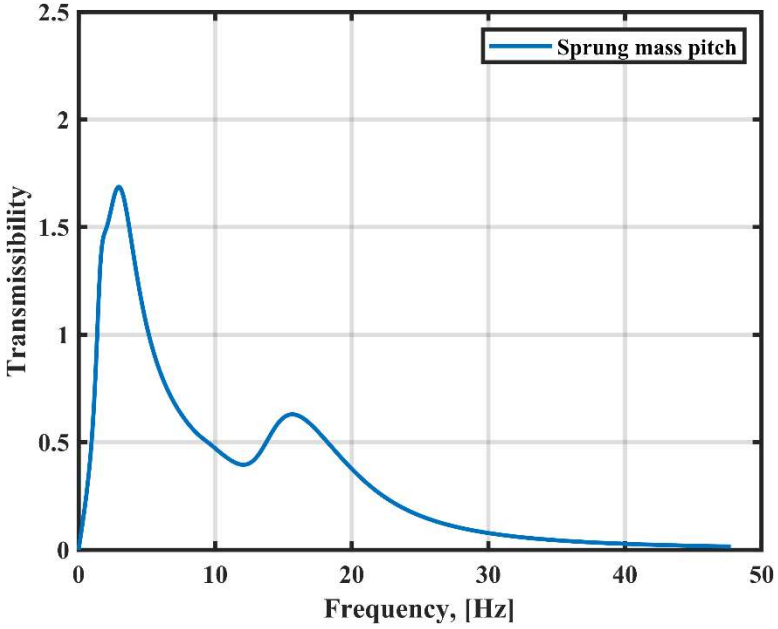

Figure B2: Eight-DOF Sprung Mass Pitch Transmissibility.

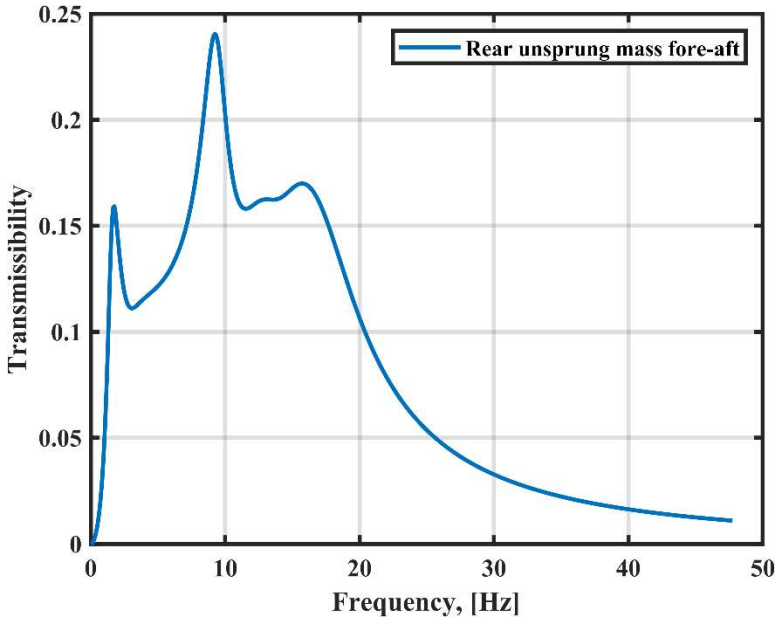

Figure B3: Eight-DOF Rear Unsprung Mass Fore-Aft Transmissibility.

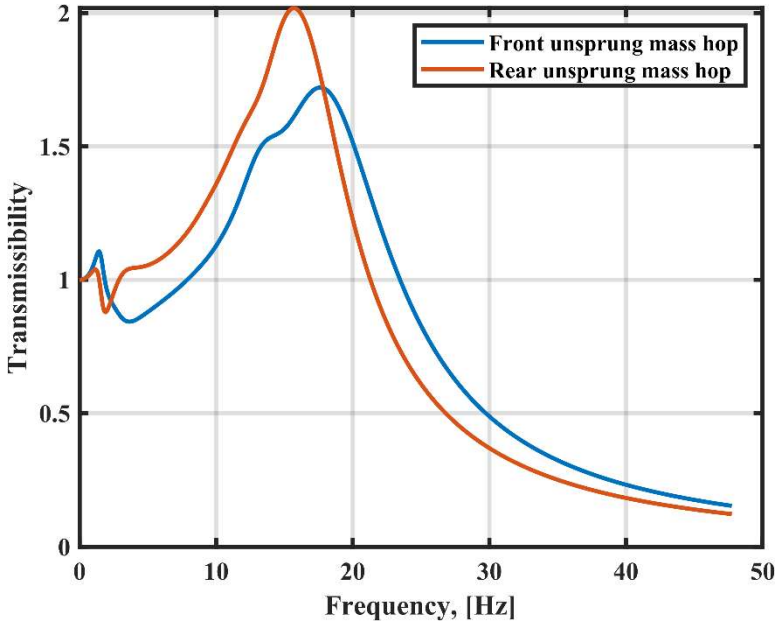

Figure B4: Eight-DOF Front and Rear Unsprung Mass Hop Transmissibility.

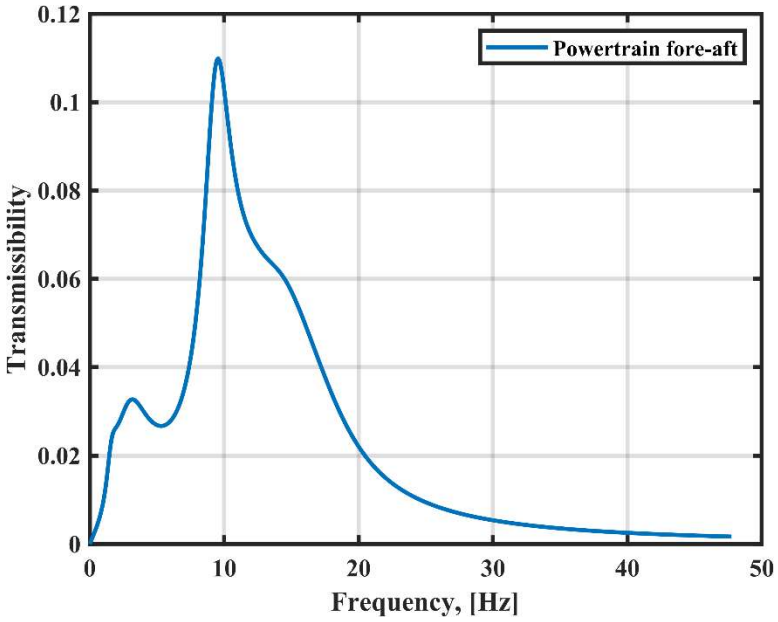

Figure B5: Eight-DOF Powertrain Fore-Aft Transmissibility.

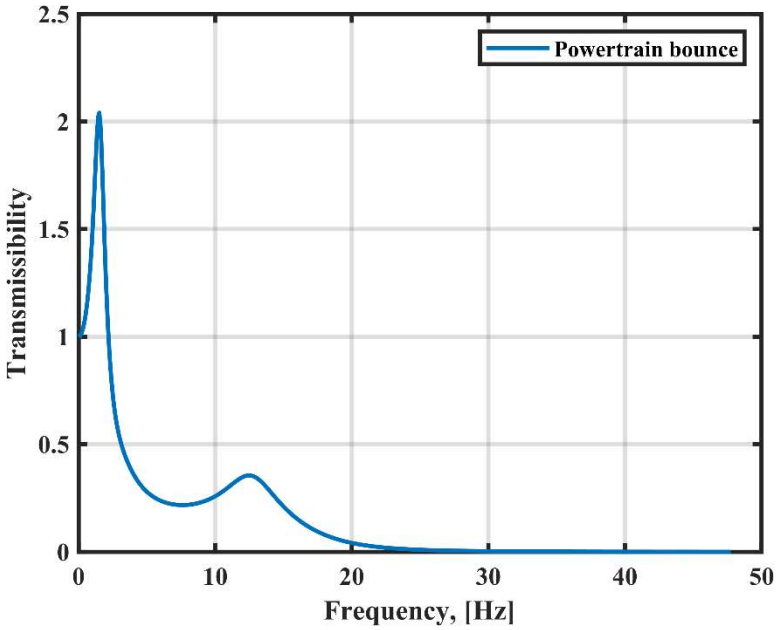

Figure B6: Eight-DOF Powertrain Bounce Transmissibility.

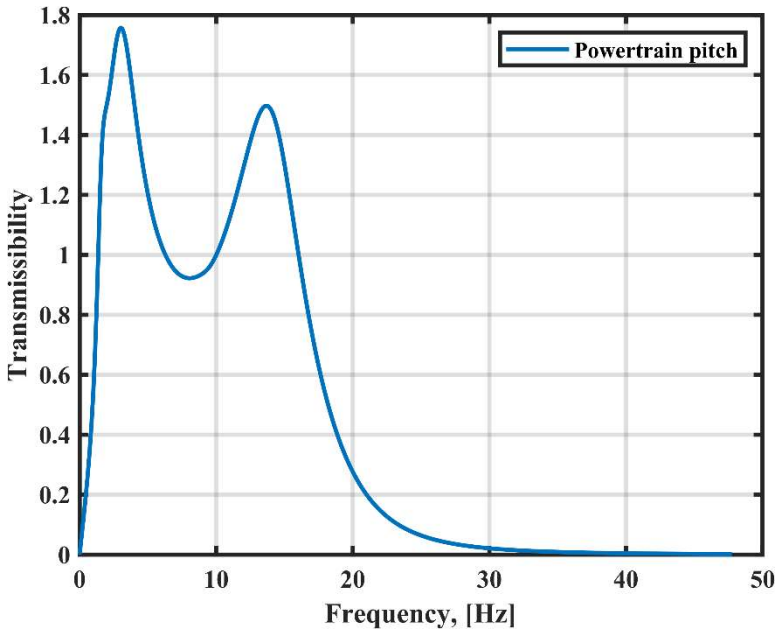

Figure B7: Eight-DOF Powertrain Pitch Transmissibility.

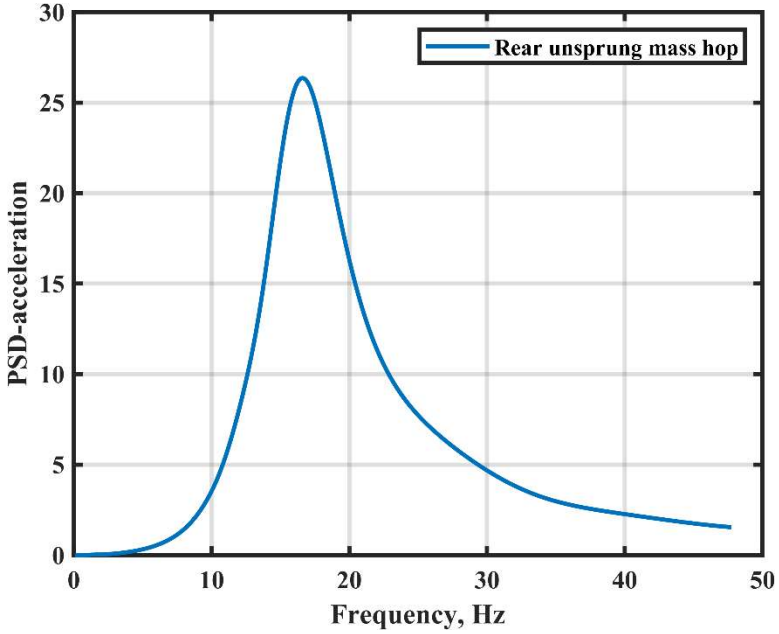

Figure B8: Eight-DOF Rear Unsprung Mass Hop PSD.

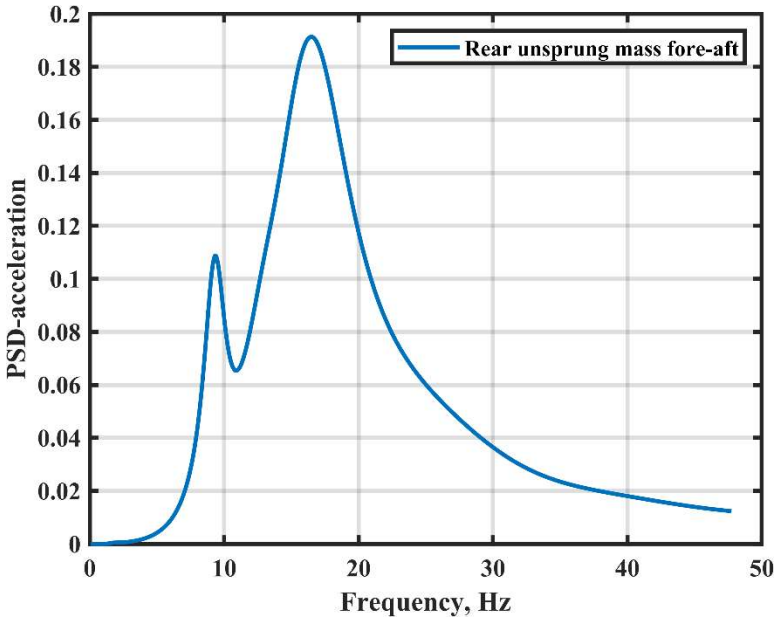

Figure B9: Eight-DOF Rear Unsprung Mass Fore-Aft PSD.

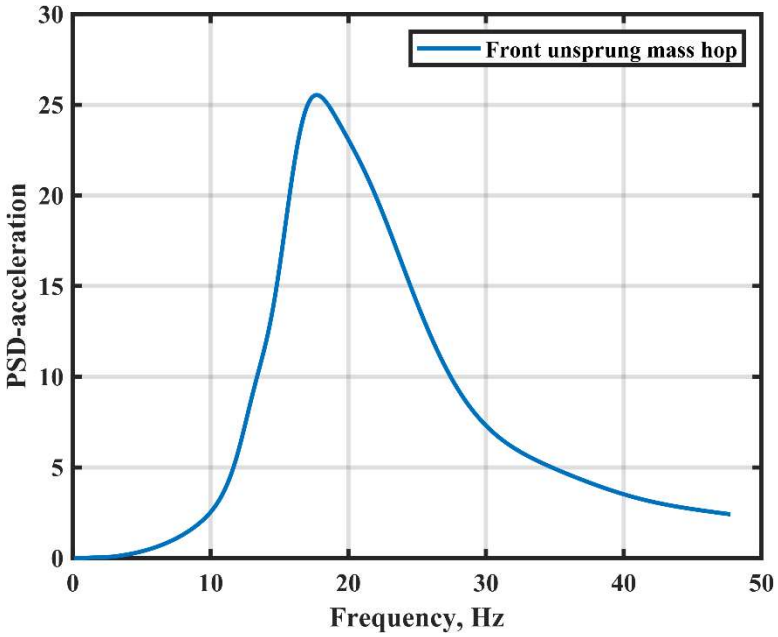

Figure B10: Eight-DOF Front Unsprung Mass Hop PSD.

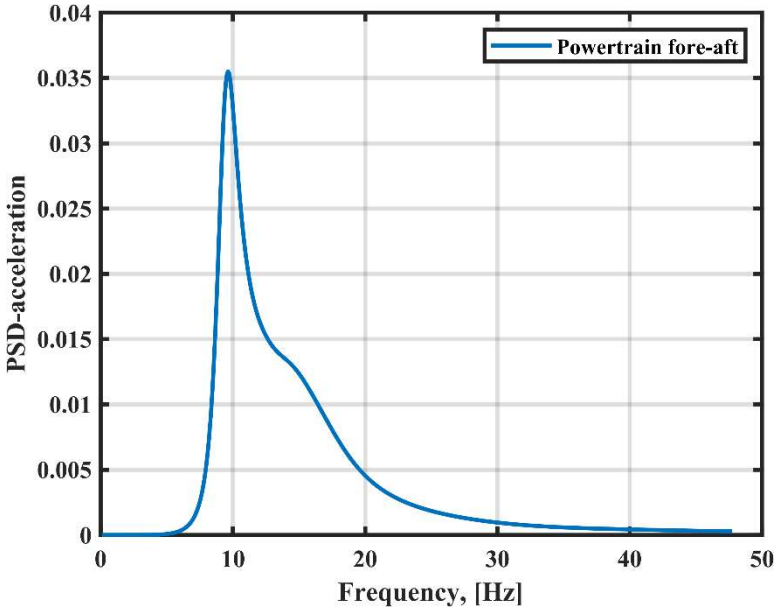

Figure B11: Eight-DOF Powertrain Fore-Aft PSD.

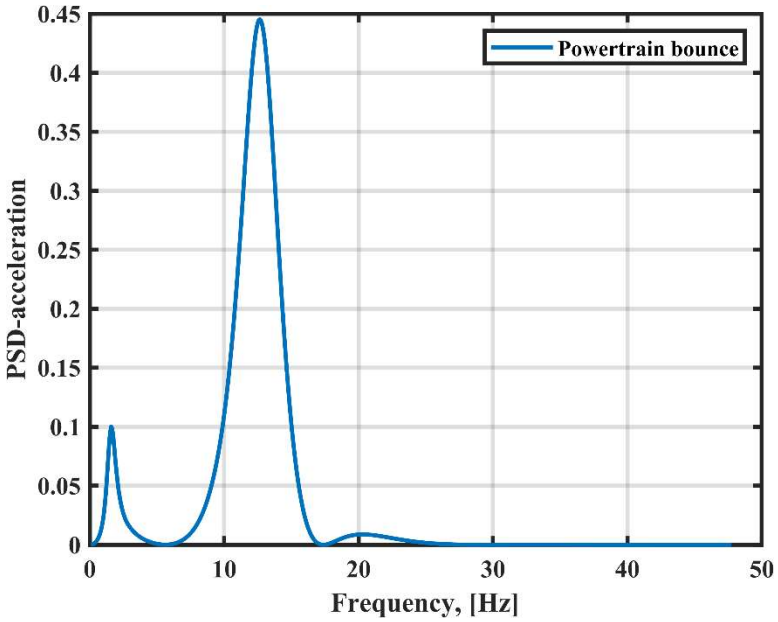

Figure B12: Eight-DOF Powertrain Bounce PSD.

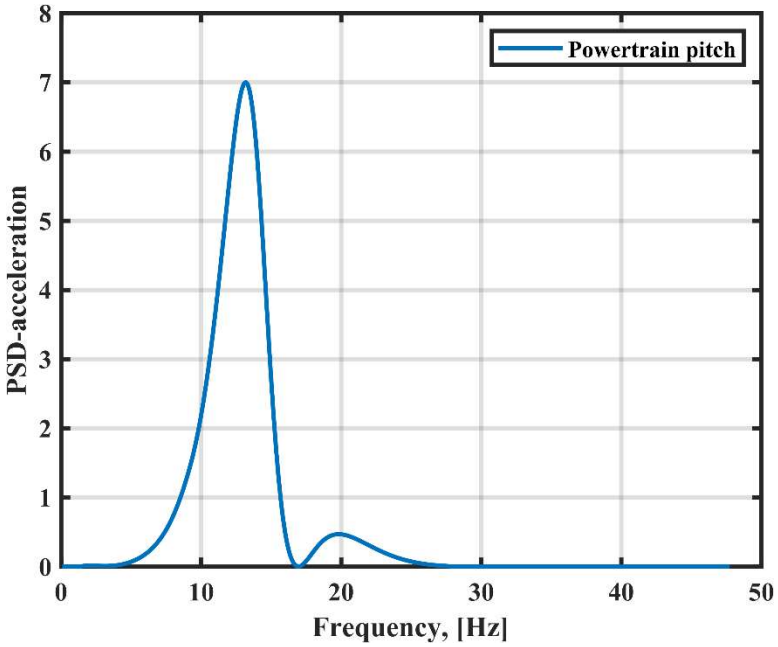

Figure B13: Eight-DOF Powertrain Pitch PSD.

Appendix C. Four-DOF MATLAB Model

```
clc
close all
clear

%Vehicle Dimensions
    p = 1.4; %Wheelbase, m
    b = 0.7; %Rear tire contact to CG, m
    v = 17; %vi*1000/3600 %vehicle steady-state speed, m/s

%Mass Matrix
    m = 325; %sprung mass, kg
    I = 38; %MOI for sprung mass, kg-m^2
    mf = 15; %front unsprung mass, kg
    mr = 18; %rear unsprung mass, kg
    M = [m 0 0 0;0 I 0 0;0 0 mf 0;0 0 0 mr];

%Equivalent vertical stiffness
kzr = 24e3; %rear shock spring coef., N/m
kzf = 15e3; %front shock spring coef., N/m
ktr = 180e3; %rear tire spring coef., N/m
ktf = 180e3; %front tire spring coef., N/m
K = [(kzf+kzr) (-kzr*b+kzf*(p-b)) (-kzf) (-kzr);...
    (-kzr*b+kzf*(p-b)) (((p-b)^2)*kzf+kzr*b^2) (-kzf*(p-b)) (kzr*b);...
    (-kzf) (-(p-b)*kzf) (kzf+ktf) 0;...
    (-kzr) (kzr*b) 0 (kzr+ktr)];

%Kp = [0 0;0 0;ktf 0;0 ktr]; %Base excitation spring matrix
Kp = [0;0;ktf;ktr];

%Equivalent vertical damping
czr = 900;%rear shock spring coef., Ns/m
czf = 900; %front shock spring coef., Ns/m
ctr = 0; %rear tire spring coef., Ns/m
ctf = 0; %front tire spring coef., Ns/m
C = [(czf+czr) (czf*(p-b)-czr*b) (-czf) (-czr);...
    (czf*(p-b)-czr*b) (((p-b)^2)*czf+czr*b^2) (-czf*(p-b)) (czr*b);...
    (-czr) ((-p+b)*czf) (czf+ctf) 0;...
    (-czr) (czr*b) 0 (czr+ctr)];
%Cp = [0 0;0 0;ctf 0;0 ctr];
Cp = [0;0;ctf;ctr];

%Transmissibility
T=[];
for w=0:0.5:300
    Tr=inv(-w^2*M+1i*w*C+K)*(Kp+1i*w*Cp);
    T=[T abs(Tr)];
End

freq=[0.1:0.5:300]/(2*pi);


%PSD
Kpp = [0 0;0 0;ktf 0;0 ktr];
Cpp = [0 0;0 0;ctf 0;0 ctr];
    Hs=[]; Srr=[];

    k0=1; S0=16e-6;% good road surface m^2/(cycle/m)
    %k0=1; S0=1024e-6;% Very Poor road surface
    for w=0:0.5:300
        Hr=-w^2*inv(-w^2*M+1i*w*C+K)*(Kpp+1i*w*Cpp);
        F=[1; exp(-1i*w*p/v)];
        Hs=[Hs Hr*F];

        if w/v <= k0
            n=2;
        else
```

```
            n=1.5;
        end

        Srr=[Srr (S0/v)*(v*k0/w)^n];
    end

w=0:0.5:300;
Sy=abs(Hs(1,:)).^2.*Srr*2*pi;
St=abs(Hs(2,:)).^2.*Srr*2*pi;
Syf=abs(Hs(3,:)).^2.*Srr*2*pi;
Syr=abs(Hs(4,:)).^2.*Srr*2*pi;

f = w/(2*pi);

%Plot Transmissibility
    w = 0:0.5:300;
    f = w/(2*pi);
    Ty = T(1,:);
    figure(1)
    plot(f,Ty)
    grid on
    ylabel('Transmissibility')
    xlabel('Frequency, [Hz]')
    legend('Sprung mass bounce')
    ylim([0;3])

    Tt = T(2,:);
    figure(2)
    plot(f,Tt)
    grid on
    ylabel('Transmissibility')
    xlabel('Frequency, [Hz]')
    legend('Sprung mass pitch')
    ylim([0;3])

    Tf = T(3,:);
    figure(3)
    plot(f,Tf)
    grid on
    ylabel('Transmissibility')
    xlabel('Frequency, [Hz]')
    legend('Front unsprung mass bounce')
    ylim([0;3])

    Tr = T(4,:);
    figure(4)
    plot(f,Tr)
    grid on
    ylabel('Transmissibility')
    xlabel('Frequency, [Hz]')
    legend('Rear unsprung mass bounce')
    ylim([0;3])



%Plot PSD
    figure(5)
    plot(f,Sy)
    grid on
    ylabel('PSD - Acceleration')
    xlabel('Frequency, Hz')
    legend('Sprung mass bounce')


    figure(6)
    plot(f,St)
    grid on
    ylabel('PSD - Acceleration')
```

```
    xlabel('Frequency, Hz')
    legend('Sprung mass pitch')

    figure(7)
    plot(f,Syf)
    hold on
    plot(f,Syr)
    grid on
    ylabel('PSD - Acceleration')
    xlabel('Frequency, [Hz]')
    legend('Front unsprung hop','Rear unsprung hop')
    hold off


%Natural Modes
[X,b] = eig(inv(M)*K);
wn = sqrt(b); %rad/s
fn = wn./(2*pi); %Hz
Cc = 2*sqrt(M*K);
zeta = C./Cc;
wd = wn.*sqrt(1-zeta.^2);

%Split eigenvectors out from solution
X1 = X(1:4,1);
X2 = X(1:4,2);
X3 = X(1:4,3);
X4 = X(1:4,4);

%Plotting mode shapes with scaled axis.
nodes = [1 2 3 4];
mode1 = transpose(X(:,1))./max(abs(transpose(X(:,1))));
mode2 = transpose(X(:,2))./max(abs(transpose(X(:,2))));
mode3 = transpose(X(:,3))./max(abs(transpose(X(:,3))));
mode4 = transpose(X(:,4))./max(abs(transpose(X(:,4))));

    figure(10)
    subplot(4,1,1)
    plot(nodes,mode1)
    hold on
    grid
    ylabel('Mode 1')
    xlabel(['Natural Mode at ',num2str(fn(1,1)),' Hz'])
    ylim([-1;1])
    set(gca, 'xtick', 0:1:4)
    subplot(4,1,2)
    plot(nodes,mode2)
    grid
    ylabel('Mode 2')
    xlabel(['Natural Mode at ',num2str(fn(2,2)),' Hz'])
    ylim([-1;1])
    set(gca, 'xtick', 0:1:4)
    subplot(4,1,3)
    plot(nodes,mode3)
    grid
    ylabel('Mode 3')
    xlabel(['Natural Mode at ',num2str(fn(3,3)),' Hz'])
    ylim([-1;1])
    set(gca, 'xtick', 0:1:4)
    subplot(4,1,4)
    plot(nodes,mode4)
    grid
    ylabel('Mode 4')
    xlabel(['Natural Mode at ',num2str(fn(4,4)),' Hz'])
    ylim([-1;1])
    set(gca, 'xtick', 0:1:4)
```

Appendix D. Eight-DOF MATLAB Model

```
clc
close all
clear


%Vehicle Dimensions
    p = 1.4; %Wheelbase, m
    b = 0.7; %Rear tire contact to CG, m
    v = 17 %vi*1000/3600 %vehicle steady-state speed, m/s

%Position of front and rear vibration isolators
    xr1 = 0.320;
    yr1 = 0.055;
    xf1 = 0.325;
    yf1 = 0.020;
%Position of swingarm connection to powertrain
    xsa = 0.270; %horizontal distance from rear tire contact point, m
    ysa = 0.030; %vertical distance from rear tire contact point, m
%Mass Inputs
    m = 200; %sprung mass, kg
    I = 38; %MOI for sprung mass, kg-m^2
    mf = 15; %front unsprung mass, kg
    mr = 18; %rear unsprung mass, kg
    mp = 125; %powertrain mass, kg
    Ip = 8; %powertrain MOI, kg-m^2
%Damping Inputs

    c1fy = 900 %front isolator equivalent vertical damping coef., Ns/m
    c1fx = 900 %front isolator equivalent horizontal damping coef., Ns/m
    c1ry = 900 %rear isolator equivalent vertical damping coef., Ns/m
    c1rx = 900 %rear isolator equivalent horizontal damping coef., Ns/m
    cpr = 0; %rear tire spring coef., Ns/m
    cpf = 0; %front tire spring coef., Ns/m
    cf = 900; %front shock equivalent damping coef., Ns/m
    cr = 900; %rear shock equivalent damping coef., Ns/m

%Stiffness Inputs
    kf = 15e3; %front shock equivalent spring coef., N/m
    kr = 24e3; %rear shock equivalent spring coef., N/m
    k1fy = 250e3; %front isolator equivalent vertical stiffness, N/m
    k1fx = 250e3; %front isolator equivalent horizontal stiffness, N/m
    k1ry = 250e3; %rear isolator equivalent vertical stiffness, N/m
    k1rx = 250e3; %rear isolator equivalent horizontal stiffness, N/m
    kpr = 180e3; %rear tire spring coef., N/m
    kpf = 180e3; %front tire spring coef., N/m

%Mass Matrix
M = zeros(8,8);
    M(1,1) = m;
    M(2,2) = I;
    M(3,3) = mf;
    M(4,4) = mr;
    M(5,5) = mr;
    M(6,6) = mp;
    M(7,7) = mp;
    M(8,8) = Ip;

%Damping Matrix
C = zeros(8,8);
    %EOM 1 Checks
    C(1,1) = cf + cr + c1fy + c1ry;
    C(1,2) = cf*(p-b) - cr*b + c1fy*xf1 - c1ry*xr1;
    C(1,3) = -cf;
    C(1,5) = -cr;
    C(1,7) = -c1fy - c1ry;
```

```
    C(1,8) = c1ry*xr1 - c1fy*xf1;
    %EOM 2 Checks
    C(2,1) = cf*(p-b) - cr*b + c1fy*xf1 - c1ry*xr1;
    C(2,2) = cf*(p-b)^2 + cr*b^2 + c1fy*xf1^2 + c1ry*xr1^2;
    C(2,3) = cf*(p-b);
    C(2,5) = cr*b;
    C(2,7) = c1ry*xr1 - c1fy*xf1;
    C(2,8) = -c1fy*xf1^2 - c1ry*xr1^2;
    %EOM 3 Checks
    C(3,1) = -cf;
    C(3,2) = -cf*(p-b);
    C(3,3) = cf + cpf;
    %EOM 4 ; NA
    %EOM 5 Checks
    C(5,1) = cr;
    C(5,2) = cr*b;
    C(5,5) = cpr + cr;
    %EOM 6 Checks
    C(6,6) = c1fx + c1rx;
    C(6,8) = c1rx*yr1 - c1fx*yf1;
    %EOM 7 Checks
    C(7,1) = -c1fy - c1ry;
    C(7,2) = -c1fy*xf1 + c1ry*xr1;
    C(7,7) = c1fy + c1ry;
    C(7,8) = c1fy*xf1 - c1ry*xr1;
    %EOM 8 Checks
    C(8,1) = -c1fy*xf1 + c1ry*xr1;
    C(8,2) = -c1fy*xf1^2 - c1ry*xr1^2;
    C(8,6) = c1rx*yr1 - c1fx*yf1;
    C(8,7) = c1fy*xf1 - c1ry*xr1;
    C(8,8) = c1fx*yf1^2 + c1fy*xf1^2 + c1rx*yr1^2 + c1ry*xr1^2;


K = zeros(8,8);
    %EOM 1
    K(1,1) = kf + kr + k1fy + k1ry;
    K(1,2) = kf*(p-b) - kr*b + k1fy*xf1 - k1ry*xr1;
    K(1,3) = -kf;
    K(1,5) = -kr;
    K(1,7) = -k1fy - k1ry;
    K(1,8) = k1ry*xr1 - k1fy*xf1;
    %EOM 2
    K(2,1) = kf*(p-b) - kr*b + k1fy*xf1 - k1ry*xr1;
    K(2,2) = kf*(p-b)^2 + kr*b^2 + k1fy*xf1^2 + k1ry*xr1^2;
    K(2,3) = -kf*(p-b);
    K(2,5) = kr*b;
    K(2,7) = k1ry*xr1 - k1fy*xf1;
    K(2,8) = -k1fy*xf1^2 - k1ry*xr1^2;
    %EOM 3
    K(3,1) = -kf;
    K(3,2) = -kf*(p-b);
    K(3,3) = kf + kpf;
    %EOM 4
    K(4,4) = 2.3712e8; %Fxr component
    K(4,5) = 0.2430e8; %Fxr component
    K(4,6) = -2.3712e8; %Fxr component
    K(4,7) = -0.243e8; %Fxr component
    K(4,8) = -2.3712e8*ysa + 0.243e8*xsa; %Fxr component
    %EOM 5
    K(5,1) = -kr;
    K(5,2) = kr*b;
    K(5,4) = 0.243e8; %Fyr component
    K(5,5) = kpr + kr + 0.0249e8; %Fyr component
    K(5,6) = -0.2430e8; %Fyr component
    K(5,7) = -0.0249e8; %Fyr component
    K(5,8) = -0.243e8*ysa + 0.0249e8*xsa; %Fyr component
    %EOM 6
    K(6,4) = -2.3712e8; %Fxsa component, xr
    K(6,5) = -0.2430e8; %Fxsa component, yr
    K(6,6) = k1fx + k1rx  + 2.3712e8;%has Fxsa component, xp
    K(6,7) = 0.2430e8; %Fxsa component, yp
```

```
    K(6,8) = k1rx*yr1 - k1fx*yf1 + 2.3712e8*ysa - 0.2430e8*xsa; %has Fxsa component,
gamma
    %EOM 7
    K(7,1) = -k1fy - k1ry;
    K(7,2) = -k1fy*xf1 + k1ry*xr1;
    K(7,4) = -0.243e8; %Fysa component, xr
    K(7,5) = -0.0249e8; %Fysa component, yr
    K(7,6) = 0.243e8; %Fysa component, xp
    K(7,7) = k1fy + k1ry + 0.0249e8; %has Fysa component, yp
    K(7,8) = k1fy*xf1 - k1ry*xr1 +0.2430e8*ysa - 0.0249e8*xsa;%has Fysa component, gamma
    %EOM 8
    K(8,1) = -k1fy*xf1 + k1ry*xr1;
    K(8,2) = -k1fy*xf1^2 - k1ry*xr1^2;
    K(8,4) = -2.3712e8*ysa + 0.2430e8*xsa; % Fxsa*ysa - Fysa*xsa component, xr
    K(8,5) = -0.2430e8*ysa + 0.0249e8*xsa; % Fxsa*ysa - Fysa*xsa component, yr
    K(8,6) = k1rx*yr1 - k1fx*yf1 + 2.3712e8*ysa - 0.2430e8*xsa; %has Fxsa*ysa component
    K(8,7) = k1fy*xf1 - k1ry*xr1 + 0.2430e8*ysa - 0.0249e8*xsa; %has Fxsa*ysa component
    K(8,8) = k1fx*yf1^2 + k1fy*xf1^2 + k1rx*yr1^2 + k1ry*xr1^2 ...
    + 2.3712e8*ysa^2 - 0.2430e8*xsa*ysa - 0.2430e8*ysa*xsa + 0.0249e8*xsa^2;%has Fxsa*ysa
- Fysa*xsa component


%Transmissibility C_prime and K_prime
Cp = [0;0;cpf;0;cpr;0;0;0];
Kp = [0;0;kpf;0;kpr;0;0;0];
%     %Front Only Excitation
%     Cp = [0;0;cpf;0;0;0;0;0];
%     Kp = [0;0;kpf;0;0;0;0;0];
%     %Rear Only Excitation
%     Cp = [0;0;0;0;cpr;0;0;0];
%     Kp = [0;0;0;0;kpr;0;0;0];

%Transmissibility
T=[];
for w=0:0.5:300
    Tr=inv(-w^2*M+1i*w*C+K)*(Kp+1i*w*Cp);
    T=[T abs(Tr)];
end

freq=[0.1:0.5:300]/(2*pi);

    %Plot Transmissibility
        w = 0:0.5:300;
        f = w/(2*pi);
        Ty = T(1,:);
        Tt = T(2,:);
        Ty_max = max(Ty);

        figure(1)
        plot(f,Ty)
        grid on
        ylabel('Transmissibility')
        xlabel('Frequency, [Hz]')
        legend('Sprung mass bounce')
        ylim([0;2.5])


        figure(2)
        plot (f,Tt)
        grid on
        ylabel('Transmissibility')
        xlabel('Frequency, [Hz]')
        legend('Sprung mass pitch')
        ylim([0;2.5])

        figure(3)
        Tf = T(3,:);
        Try = T(5,:);
        Tf_max = max(Tf);
```

```
        plot(f,Tf)
        hold on
        plot(f,Try)
        hold off
        grid on
        ylabel('Transmissibility')
        xlabel('Frequency, [Hz]')
        legend('Front unsprung mass hop','Rear unsprung mass hop')


        figure(4)
        Trx = T(4,:);
        plot(f,Trx)
        grid on
        ylabel('Transmissibility')
        xlabel('Frequency, [Hz]')
        legend('Rear unsprung mass fore-aft')

        figure(5)
        Tpx = T(6,:);
        plot(f,Tpx)
        grid on
        ylabel('Transmissibility')
        xlabel('Frequency, [Hz]')
        legend('Powertrain fore-aft')

        figure(6)
        Tpy = T(7,:);
        plot (f,Tpy);
        grid on
        ylabel('Transmissibility')
        xlabel('Frequency, [Hz]')
        legend('Powertrain bounce')

        figure(7)
        Tpt = T(8,:);
        plot (f,Tpt);
        grid on
        ylabel('Transmissibility')
        xlabel('Frequency, [Hz]')
        legend('Powertrain pitch')



%PSD
Kpp = [0 0;0 0;kpf 0;0 0;0 kpr;0 0;0 0;0 0];
Cpp = [0 0;0 0;cpf 0;0 0;0 cpr;0 0;0 0;0 0];
Hs=[]; Srr=[];

k0=1; S0=16e-6;% good road surface m^2/(cycle/m)
%k0=1; S0=1024e-6;% Very Poor road surface
for w=0:0.5:300
    Hr=-w^2*inv(-w^2*M+1i*w*C+K)*(Kpp+1i*w*Cpp);
    F=[1; exp(-1i*w*p/v)];
    Hs=[Hs Hr*F];

    if w/v <= k0
        n=2;
    else
        n=1.5;
    end

    Srr=[Srr (S0/v)*(v*k0/w)^n];
end

w=0:0.5:300;

Sy=abs(Hs(1,:)).^2.*Srr;
```

```
St=abs(Hs(2,:)).^2.*Srr;
Syf=abs(Hs(3,:)).^2.*Srr;
Sxr=abs(Hs(4,:)).^2.*Srr;
Syr=abs(Hs(5,:)).^2.*Srr;
Sxp=abs(Hs(6,:)).^2.*Srr;
Syp=abs(Hs(7,:)).^2.*Srr;
Sgp=abs(Hs(8,:)).^2.*Srr;
S = [Sy;St;Syf;Sxr;Syr;Sxp;Syp;Sgp];

f = w/(2*pi);

    figure(8)
    plot(f,Sy)
    grid on
    ylabel('PSD-acceleration')
    xlabel('Frequency, Hz')
    legend('Sprung mass bounce')

    figure(9)
    plot(f,St)
    grid on
    ylabel('PSD-acceleration')
    xlabel('Frequency, Hz')
    legend('Sprung mass pitch')

    figure(10)
    plot(f,Syf)
    grid on
    ylabel('PSD-acceleration')
    xlabel('Frequency, Hz')
    legend('Front unsprung mass hop')

    figure(11)
    plot(f,Sxr)
    grid on
    ylabel('PSD-acceleration')
    xlabel('Frequency, Hz')
    legend('Rear unsprung mass fore-aft')

    figure(12)
    plot(f,Syr)
    grid on
    ylabel('PSD-acceleration')
    xlabel('Frequency, Hz')
    legend('Rear unsprung mass hop')

    figure(13)
    plot(f,Sxp)
    grid on
    ylabel('PSD-acceleration')
    xlabel('Frequency, [Hz]')
    legend('Powertrain fore-aft')

    figure(14)
    plot(f,Syp)
    grid on
    ylabel('PSD-acceleration')
    xlabel('Frequency, [Hz]')
    legend('Powertrain bounce')

    figure(15)
    plot(f,Sgp)
    grid on
    ylabel('PSD-acceleration')
    xlabel('Frequency, [Hz]')
    legend('Powertrain pitch')
```

```
%Natural Modes
[X,L] = eig(inv(M)*K);
%L = eig(inv(M)*K);
wn = sqrt(L); %rad/s
fn = wn./(2*pi); %Hz
Cc = 2*sqrt(M*K);
zeta = C./Cc;
wd = wn.*sqrt(1-zeta.^2);

%Mode Shapes
X1 = X(1:8,1);
X2 = X(1:8,2);
X3 = X(1:8,3);
X4 = X(1:8,4);
X5 = X(1:8,5);
X6 = X(1:8,6);
X7 = X(1:8,7);
X8 = X(1:8,8);

    %Scale Mode Shapes
    X1_R = X1/max(abs(X1));
    X2_R = X2/max(abs(X2));
    X3_R = X3/max(abs(X3));
    X4_R = X4/max(abs(X4));
    X5_R = X5/max(abs(X5));
    X6_R = X6/max(abs(X6));
    X7_R = X7/max(abs(X7));
    X8_R = X8/max(abs(X8));

%Plotting mode shapes with scaled axis.
nodes = [1 2 3 4 5 6 7 8];

    figure(16)
    subplot(8,1,1)
    plot(nodes,X1_R)
    hold on
    grid
    ylabel('Mode 1')
    xlabel(['Natural Mode at ',num2str(fn(1,1)),' Hz'])
    ylim([-1;1])
    set(gca, 'xtick', 0:1:8)

    subplot(8,1,2)
    plot(nodes,X2_R)
    grid
    ylabel('Mode 2')
    xlabel(['Natural Mode at ',num2str(fn(2,2)),' Hz'])
    ylim([-1;1])
    set(gca, 'xtick', 0:1:8)

    subplot(8,1,3)
    plot(nodes,X3_R)
    grid
    ylabel('Mode 3')
    xlabel(['Natural Mode at ',num2str(fn(3,3)),' Hz'])
    ylim([-1;1])
    set(gca, 'xtick', 0:1:8)

    subplot(8,1,4)
    plot(nodes,X4_R)
    grid
    ylabel('Mode 4')
    xlabel(['Natural Mode at ',num2str(fn(4,4)),' Hz'])
    ylim([-1;1])
    set(gca, 'xtick', 0:1:8)

    subplot(8,1,5)
    plot(nodes,X5_R)
```

```
grid
ylabel('Mode 5')
xlabel(['Natural Mode at ',num2str(fn(5,5)),' Hz'])
ylim([-1;1])
set(gca, 'xtick', 0:1:8)

subplot(8,1,6)
plot(nodes,X6_R)
grid
ylabel('Mode 6')
xlabel(['Natural Mode at ',num2str(fn(6,6)),' Hz'])
ylim([-1;1])
set(gca, 'xtick', 0:1:8)

subplot(8,1,7)
plot(nodes,X7_R)
grid
ylabel('Mode 7')
xlabel(['Natural Mode at ',num2str(fn(7,7)),' Hz'])
ylim([-1;1])
set(gca, 'xtick', 0:1:8)

subplot(8,1,8)
plot(nodes,X8_R)
grid
ylabel('Mode 8')
xlabel(['Natural Mode at ',num2str(fn(8,8)),' Hz'])
ylim([-1;1])
set(gca, 'xtick', 0:1:8)
```

Engineering

Capstone Report Approval Form

Master of Science in Engineering – MSE

Milwaukee School of Engineering

This capstone report, titled "Sensitivity of Ride Comfort of a Motorcycle to the Rear Powertrain Mounting System," submitted by the student Brennan Long, has been approved by the following committee:

Faculty Advisor: Sudhir Kaul Date: 05/20/2025

Dr. Sudhir Kaul, Ph.D.

Faculty Member: M.M.Falah Date: 5/19/2025

Dr. Mohammad Mahinfalah, Ph.D.

Faculty Member: Gary Shimek Date: 5/20/2025

Professor Gary Shimek, M.L.I.S.